EUROfusion

WPDTT2-PR(17) 18099

A Loarte et al.

Power exhaust in tokamaks and scenario integration issues

Preprint of Paper to be submitted for publication in
Fusion Engineering and Design

This work has been carried out within the framework of the EUROfusion Consortium and has received funding from the Euratom research and training programme 2014-2018 under grant agreement No 633053. The views and opinions expressed herein do not necessarily reflect those of the European Commission.

Power exhaust in tokamaks and scenario integration issues

A. Loarte[1] and R. Neu[2]

[1]ITER Organization, Route de Vinon-sur-Verdon - CS 90 046, 13067 St Paul Lez Durance, France

[2]Max-Planck-Institut für Plasmaphysik, Boltzmannstraße 2, D-85748 Garching, Germany

Abstract. A review of the main concepts, proposed solutions and results of R&D as well as outstanding issues on power exhaust in tokamaks is presented with specific emphasis on the expected issues that need to be resolved for ITER and future fusion reactors such as DEMO for both conventional and advanced divertor concepts.

1. Introduction

The achievement of fusion production in tokamak reactors can only be realized through the integration of DT plasmas with thermonuclear characteristic (achievement of T > 10 keV and $nT\tau_E \sim 10^{22}$ $m^{-3}keVs$) with power and particle fluxes to the reactor vessel which are compatible with the power handling capabilities and erosion lifetime of the components that protect it (plasma facing components or PFCs). In turn, the erosion of the plasma facing components generates impurities that can enter the confined plasma and decrease fusion power production by DT fuel dilution and increased electromagnetic radiative losses. In addition the helium ash from DT reactions must be removed by the plasma to avoid DT fuel dilution and this must be achieved within a given total fuel throughput to limit the amount of tritium that is required for the operation of the fusion reactor. These integration issues already have to be addressed to maintain plasma performance in the present generation of experiments, particularly those operating with high Z PFCs [Neu 2005, Romanelli 2013, Greenwald 2014] with DT plasmas [Horton 1999, Strachan 1997]. Moreover, the successful resolution of such integration issues is essential for the success of ITER, presently under construction, DEMO and future fusion power plants given the significantly larger edge power and particle fluxes and duration of plasma discharges (from several minutes to continuous operation). These large particle and power fluxes and the long duration of the plasma discharges requires that the PFCs are actively cooled; this limits the power fluxes that can be deposited by the plasma (≤ 10 MWm^{-2}) on the PFCs [Merola 2002] and the thickness of the PFCs themselves (≤ 1 cm) [Hirai 2013] and thus their erosion lifetime.

Extensive R&D carried out in present tokamaks to resolve the challenges of particle and power exhaust has already provided the basic concepts on which the designs of ITER and DEMO are based:

- the modification of the magnetic field at the edge plasma by coils external to the plasma which creates a magnetic separatrix in which the poloidal magnetic field is zero at one or more points (so called poloidal divertor configuration and X-points respectively see Fig. 1). This separates the region of interaction between the confined thermonuclear plasma, through a region of open field lines or scrape-off layer (SOL), and the PFCs and allows the reduction of the power flux on the PFCs (so-called divertor targets) and the increase of particle exhaust by the establishment of high density and low temperature conditions in the divertor plasma itself.

- the use of metallic PFCs, in particular made of tungsten (W), for the divertor targets which are subject to high fluxes, which do not form strongly bound chemical compounds with

hydrogenic isotopes and thus prevent T to be trapped in the reactor vessel [Roth 2008]. While this PFC choice is not directly linked with the general problem of power and particle exhaust it leads to specific issues due to the erosion of the materials resulting from the interaction with the plasma and to the very small amounts of W which can be tolerated in thermonuclear plasmas due to its large electromagnetic radiation efficiency [Kallenbach 2005]. It should be pointed out that another potential solution to the power exhaust problem is based on the use of liquid metals which has potential advantages with respect to erosion lifetime and, potentially allows the achievement of power handling capabilities in excess of 10 MWm^{-2}. This approach presents specific issues regarding plasma-wall interactions and the interaction of liquid metals with magnetic fields that will be not be discussed here; the reader is referred to [Mazitelli 2015] for details on this topic.

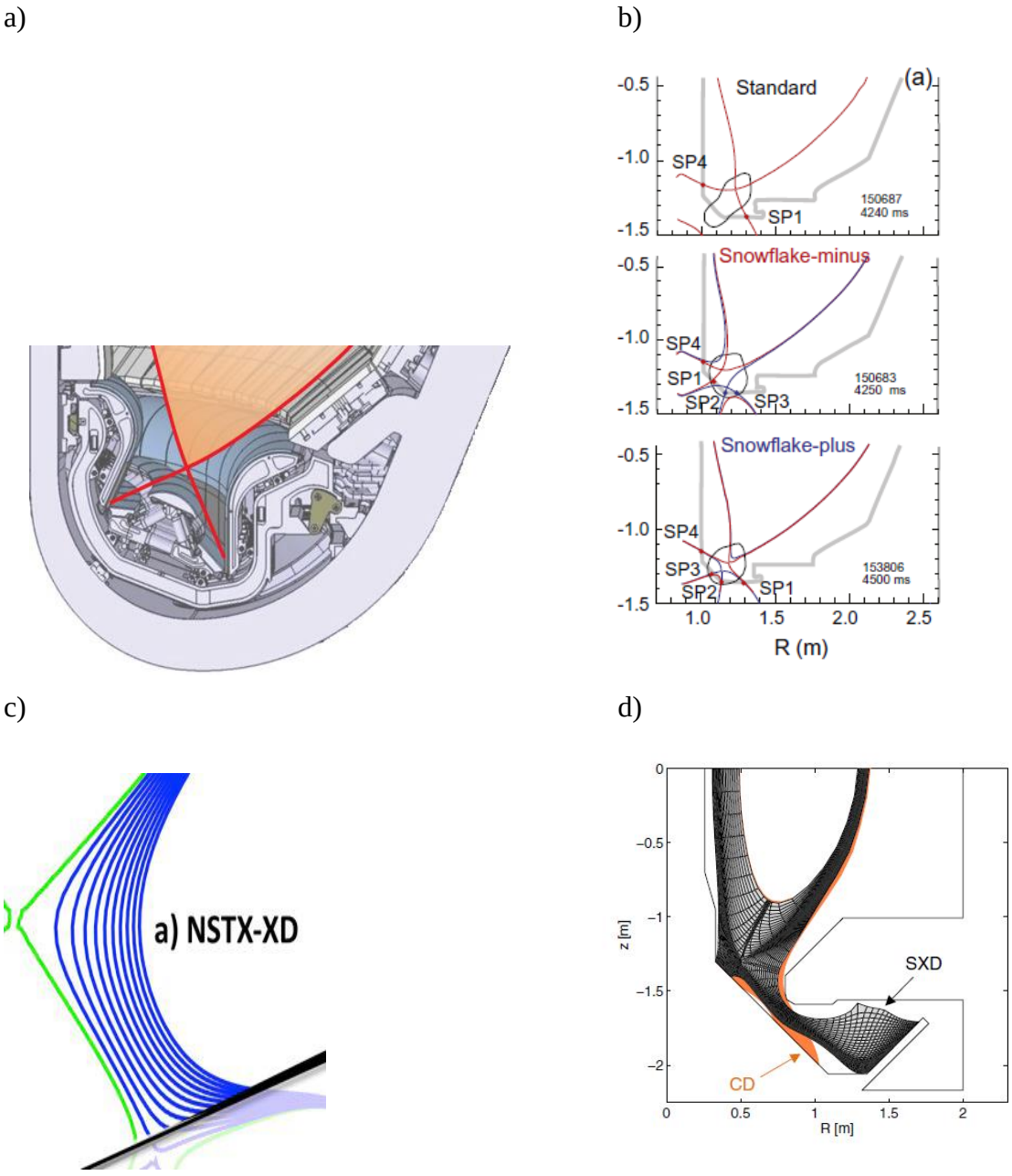

Figure 1. Magnetic configuration of a conventional vertical divertor and various advanced divertor configurations: a) ITER vertical divertor (conventional) [Pitts 2013], b) Snowflake

divertor configurations in DIII-D [Soukhanovskii 2015], c) Super-X divertor in MAST-U [Havlíčková 2014] and d) X divertor in NSTX [Kotschenreuther 2013].

In this paper we review the basic concepts for power and particle exhaust in tokamaks and progress in R&D to address the integration issues mentioned above. We also highlight the remaining challenges that need to be resolved for DEMO both in ITER and other smaller scale devices where the conventional divertor and advanced divertor approaches to this challenge will be investigated. The paper is structured as follows: section 2 addresses first the basic issues related to power exhaust in tokamaks and the consequences of divertor geometry on this, section 3 describes the dissipative processes that are utilized to decrease the divertor power flux level, section 4 describes the use of dissipative processes in the confined plasma to ease the divertor power exhaust problem, section 5 discusses issues related to the compatibility of power exhaust and particle exhaust and finally section 6 summarises the conclusions.

2. Edge power flow characteristics in present tokamaks and fusion reactors

The so-called power exhaust problem in tokamaks is caused by the large difference in the rate of transport of plasma energy across and along the magnetic field lines. The magnetic field provides very good thermal insulation and leads to a very low effective heat diffusivity across the magnetic field that provides the energy confinement required for the achievement of thermonuclear temperatures in fusion reactors. On the other hand, magnetic fields do not have an effect on the heat diffusivity of the plasma along the field line, as the magnetic forces on charged particles along the magnetic field are zero. Thus heat transport in the open field lines or SOL is much faster than across the field and this leads to the power being lost by the confined plasma to be deposited in a very small area; typically this area is few tenths of percent of the total area of the PFCs. For ITER and DEMO, in which the power lost by the confined plasma by conduction and convection is hundreds of MWs and the area of the PFCs is ~ 1000 m^2, this leads to power fluxes at the divertor targets far above the engineering design limits of ~ 10 MWm^{-2}.

Power exhaust in tokamaks becomes more challenging with increasing tokamak size and pulse length duration, in particular, in fusion reactors with dominant alpha heating. This is the result of two factors:

a) As a consequence of MHD stability and other empirical operational limits (i.e. plasma density being limited by the Greenwald scaling [Greenwald 2002]) and of the energy confinement scaling for plasmas in the high confinement mode (H-mode) [ITER Physics Basis 2007], the thermal energy of the plasma increases with the size of the tokamak as $W_{th} \sim R^{4-5}$. Thus, for thermonuclear temperatures, the alpha power that needs to be exhausted by the PFCs scales as $P_\alpha \sim W_{th}^2 \sim R^{8-10}$. This leads to typical values of thermal energies in the largest existing tokamaks such as JET of ~ 10-15 MJ [Horton 1999] while is expected to be > 300 MJ in ITER [ITER Physics Basis 2007] and DEMO [Wenninger 2015] and correspondingly the maximum stationary alpha power production achieved at JET has reached ~ 1 MW while is its expected to reach ≥ 100 MW in ITER and DEMO.

b) The effective area of the PFCs on which the power outflow is deposited is not expected to increase significantly with the size of the device. This is the result of the scaling of plasma transport at the plasma edge for the H-mode regime that provides the energy confinement required for the achievement of high fusion gain in reactors [Wagner 1982], in which a region with very low heat diffusivity is formed at the edge of the confined plasma where turbulent

transport is suppressed (edge transport barrier or ETB). While this confinement regime is essential for the design of tokamak reactors, recent models [Goldston 2012] and experimental R&D [Eich 2013] has shown that it has significant implication for the expected level of edge heat diffusivity and for power exhaust. This is due to the fact that the suppression of turbulent transport at the edge of the confined plasma extends to the near-SOL region where field lines are open and the resulting heat diffusivity in this region, leads to an unfavourable scaling with device size. Indeed the width (in minor plasma radius) over which the power flux is deposited on the PFCs (λ_q) for H-mode plasmas is found to scale as Eq. 1 [Goldston 2012], which is describes well the experimental findings across a large range of devices (see Fig. 2).

$$\lambda_q \sim \frac{\sqrt{2kT/m_i}}{eB_p} = \frac{qR}{aeB_t}\sqrt{2kT/m_i} \qquad (1)$$

where T is the plasma temperature at the magnetic separatrix, q is the edge safety factor, R and a are the major and minor radii, respectively and B_t is the toroidal field. This leads to the effective area for power deposition on the PFCs to scale as

$$A_{PFC} = 2\pi R\lambda_q = \frac{2\pi qR}{ae}\frac{R}{B_t}\sqrt{2kT/m_i} \qquad (2)$$

For typical operation in tokamaks with R/a = 3 and q ~ 3 this leads to less than linear dependence of A_{PFC} on R (i.e. R/B_t scales less weakly than R) given the fact that T scales weakly with R, as it is determined by heat transport along the field for which plasma conductivity increases strongly with T ($\kappa \sim T^{5/2}$).

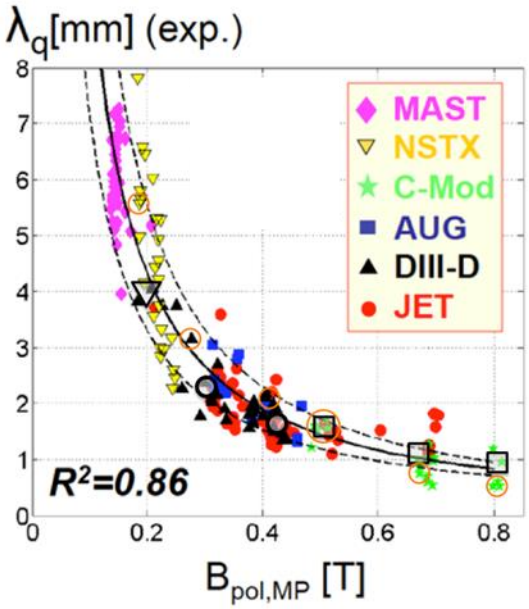

Figure 2. Measured SOL power flow decay length versus poloidal magnetic field at the separatrix for a range of experiments in present tokamak devices [Eich 2013].

The magnetic geometry of the divertor by itself can be used to increase this effective area for power deposition by taking advantage of the characteristics of plasma transport along the field and across the field within the divertor itself. This is done by:

a) Modifying the magnetic flux expansion at the divertor target by: modifying the poloidal magnetic field around the X-point (poloidal flux expansion), locating the divertor target at large R (toroidal flux expansion) and/or by the design of the divertor target. These approaches can decrease the power flux along the field at the divertor

target (Eq. 3) and the power flux onto the divertor target itself (see Eq. 4) if the normal component of the magnetic field line on the target decreases (this depends both on magnetic field and target geometric design).

$$q_{\parallel-div} = P_{SOL}/(2\pi R \frac{B_p}{B_t} \lambda_q) \quad (3)$$

$$q_{\perp-div} = q_{\parallel-div} \sin(\frac{B_p^{norm}}{B_t}) \quad (4)$$

It should be noted that the decrease of the angle of incidence of the field lines at the divertor target is limited by the accuracy of installation and alignment of the plasma facing components themselves to angles typically larger than 2-3^o in next step tokamak fusion reactors where these components have to be installed/replaced by remote handling [Merola]. For very low incidence angles, the field lines can run almost parallel to the divertor target in the toroidal direction and this leads to either perpendicular field line impact on misaligned PFCs, with stationary power fluxes > 100 MWm^{-2}, or to a large decrease of the effective length (and of effective area) for power deposition of the divertor PFCs in the toroidal direction when these are designed to hide misaligned PFCs.

b) by taking advantage of anomalous transport in the divertor itself, particularly in the regions not connected to the main scrape-off layer (so-called private flux region or PFR). This decreases the value of $q_{||\text{-div}}$ by heat transport into the private flux region which receives no direct power flux from the main plasma and is significant when the length of the field lines in the divertor region is not negligible compared to that in the SOL.

In the conventional divertor approach (Fig. 1.a), the X-point is created by a quadrupole field with the poloidal magnetic field increasing linearly with the distance to the X-point. In this configuration there are two possibilities to increase the magnetic flux expansion and reduce the angle of incidence of the field line at the divertor target one is by locating the X-point very close to the target and the other by inclining the divertor with respect to the magnetic field, thus increasing the effective flux expansion and decreasing the incidence angle even for a distant X-point, as shown in Fig. 1.a. The second option is found to be more advantageous, as it separates more effectively the confined plasma from the divertor impurity source and allows the increase of radiative losses in the divertor volume while maximizing the decrease of q_{div} by heat transport in the PFR. An example of this effect for the ITER divertor in conditions with low atomic/radiative losses is shown in Fig. 3 [Loarte 2015a], where a factor of more than 2 in the divertor heat flux reduction can be accounted for by heat diffusion into the PFR.

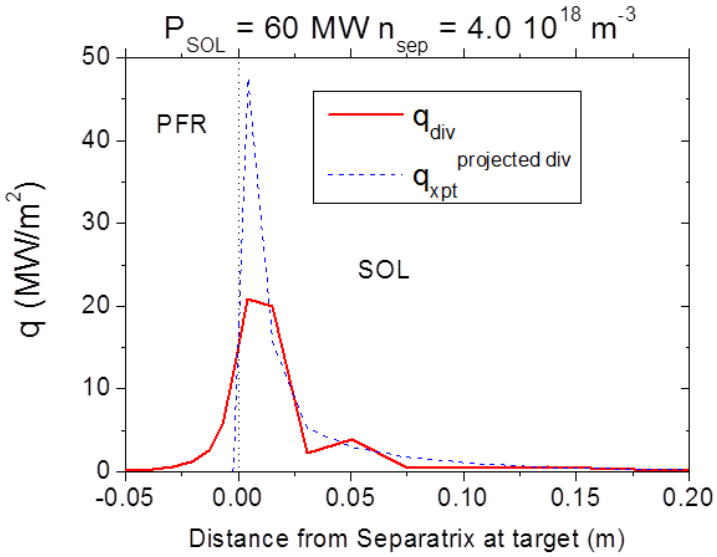

Figure 3. Power flux at the outer divertor target for an ITER SOLPS simulation with P_{SOL} = 60 MW and separatrix density n_{sep} = 4 10^{18} m^{-3}. The red-full line corresponds to the modelled divertor target power flux while the blue-dashed line corresponds to the expected power flux at the divertor target in the absence of diffusion in the private flux region, as evaluated by projecting the parallel power flux at the divertor entrance onto the divertor target [Loarte 2015a].

Advanced divertors take advantage of both the flux expansion modification and the diffusion in the PFR to decrease the divertor power flux with the main features achieved depending on the magnetic configuration chosen:

- Snowflake divertor (Fig. 1.b). In this magnetic configuration, the X-point is created by a higher order null which can increase the number of strike points of the magnetic separatrix at the divertor target up to four and the number private flux regions at the divertor up to to three. Depending on whether the configuration is a pure snowflake or not and on the distance between the X-point and the divertor target this configuration can provide a large magnetic flux expansion at the target or not. In addition to the effects above, it is also expected that the large region with low magnetic field near the X-point(s) in this configuration can increase anomalous transport in the divertor thus decreasing $q_{||\text{-div}}$ beyond the expectations from the sharing of power among the four strike points and the diffusion into the three private flux regions [Reimerdes 2013].

- X divertor (Fig. 1.c). In this configuration the flux expansion near the divertor target is increased by the creation of local magnetic fields near the divertor targets; this increases the wetted area for power deposition and decreases the incidence angle of the magnetic field line on the target. The effect of heat diffusion into the private flux region can also be increased if the length of the field lines in the divertor region is significantly increased.

- Super-X divertor (Fig. 1.d). In this configuration the poloidal length of the field line in the divertor is extended and the intersection with the divertor target is moved to large a location with a major radius significantly larger than the magnetic axis $R_{div}/R_{mag} >> 1$. In addition, a local modification of the magnetic flux expansion near the divertor target, similar to the X-divertor, is also applied. The extended length of the field line increases greatly the diffusion of heat in the PFR thus decreasing $q_{||\text{-div}}$. In addition, the large R_{div}/R_{mag} decreases the value of the B_t at the divertor target (B_t ~1/R) which also decreases $q_{||\text{-div}}$ due to the increased area for heat flux along the magnetic field with decreasing B_t (see Eq. 3). The reduction of B_t, on the

other hand, increases the incidence angle of the field line on the target thus increasing the power flux projected on the target and compensating to some degree the reduction $q_{\|\text{-div}}$ by this effect (see Eq. 4). It is therefore important to ensure by both divertor target design and local modification of the poloidal field near the target that the angle of incidence of the field line on the divertor target remains low to take full advantage of the benefits provided by the decreased toroidal field and increased toroidal flux expansion at the divertor target provided by this configuration.

In addition to these effects which are purely related to the divertor magnetic geometry, the advanced divertor geometries are also expected to have favourable features for the access to high density and low temperature divertor plasma conditions that are required to reduce further the power flux at the divertor target in DEMO by electromagnetic radiation and other atomic losses which is discussed in the next section.

3. Radiative divertors and detachment

To reduce the magnitude of the power fluxes at the divertor target beyond what can be achieved by divertor magnetic geometry and the associated heat transport within the divertor itself it is necessary to dissipate the power by other means than plasma transport over a larger area of the PFCs. This can be achieved by increasing the ionization and electromagnetic losses by impurities and re-ionizing neutrals in the divertor plasma. These atomic processes and electromagnetic radiation tend to lead to isotropic losses from the plasma thus spreading the power lost by the plasma over a much larger area than when it flows along the magnetic field thus greatly reducing the local power fluxes on PFCs. The local re-ionization of hydrogenic ions (H, D or T) from the plasma which are neutralized at the divertor target increases the divertor plasma density and decreases its temperature achieving the so-called high recycling divertor regime in which the local ionization source in the divertor plasma volume is much larger than the particle outflow from the confined plasma. In this regime the divertor temperature and density change with separatrix density as [Loarte 1998]:

$$n_{\mathrm{d}} = \left(\frac{7\gamma L_{\mathrm{c}}}{8\kappa_0\sqrt{m_{\mathrm{i}}}}\right)^2 \frac{n_{\mathrm{s}}^3}{T_{\mathrm{s}}^4} \tag{5}$$

$$T_{\mathrm{d}} = \frac{1}{2}\left(\frac{8\kappa_0\sqrt{m_{\mathrm{i}}}}{7\gamma L_{\mathrm{c}}}\right)^2 \frac{T_{\mathrm{s}}^5}{n_{\mathrm{s}}^2} \tag{6}$$

Where L_c is the length of the field lines in the SOL and n_s is the separatrix density and T_s the separatrix temperature given by:

$$T_{\mathrm{s}} = \left(\frac{7L_{\mathrm{c}}^2}{4\kappa_0(2\pi R)(2\pi a)\lambda_{\mathrm{q}}}\right)^{2/7} (P_{\mathrm{sol}})^{2/7} \tag{7}$$

where P_{SOL} is edge power flow from the confined plasma.

For sufficiently large n_s the divertor density can significantly exceed the density in the confined plasma and a large gradient in plasma temperature is established along the separatrix from the vicinity of the confined plasma to the divertor. It should be noted that in the absence of large radiative losses from the recycling neutrals and impurities the peak heat flux to the divertor is not significantly decreased when n_s increases as $q_{div} \sim n_d T_d^{3/2}$ in these conditions.

The inclusion of impurities (intrinsic for carbon-based PFCs or extrinsic for high Z PFCs) adds a significant channel for increased power losses in the divertor plasma. In coronal approximation their radiation efficiency ($L_z(T_e)$ as shown in Fig. 4), is large at low divertor temperatures and the radiated power density, given by $P_{rad} = C_z n_e^2 L_z(T_e)$, increases with n_e^2 for a given impurity concentration C_z. In general, the radiation efficiency is further increased through transport (or the finite confinement time) of the impurities. This leads to a significant increase of radiative power losses in the conditions of high density and temperature achieved by the high recycling regime and to a significant decrease of the divertor power flux.

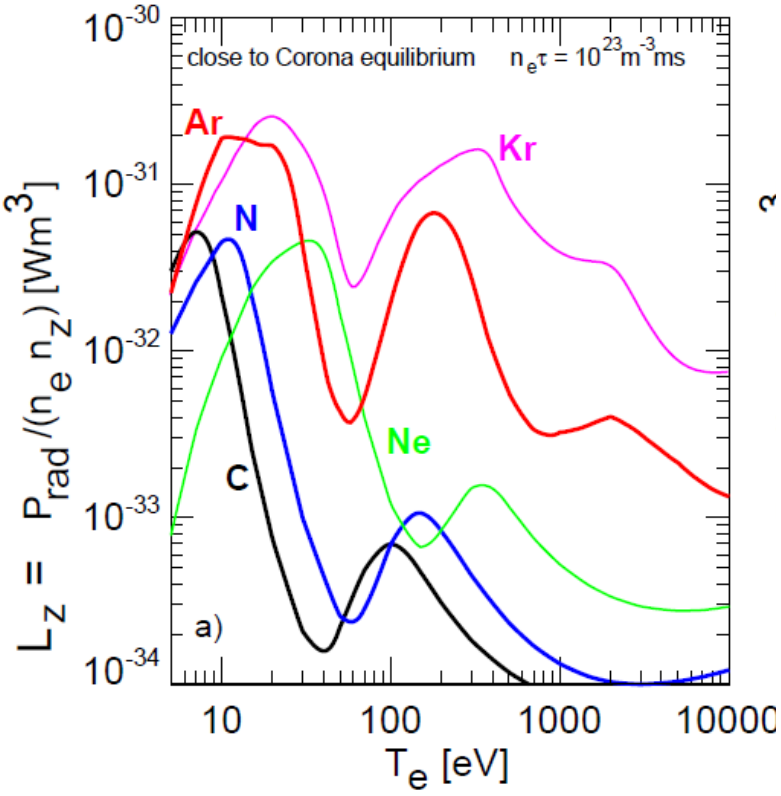

Figure 4. Radiation efficiency for hydrogen and a range of impurities from the ADAS database. The dashed lines correspond to Bremsstrahlung radiation [Kallenbach 2013].

However, in the absence of additional physics processes, the reduction of the power flux at the divertor is limited to values of ~ 50% [McCracken 1993]. This is due to the fact that in the high recycling divertor regime there is no loss of momentum or particles at the divertor and this leads to the power flux at the divertor to depend on separatrix density and temperature and divertor temperature as:

$$q_{\parallel-div} = n_{div} c_{s-div} (\gamma + E_H) = \sqrt{\frac{1}{2m}} n_s T_s \left(\gamma \sqrt{T_d} + \frac{E_H}{\sqrt{T_d}} \right) \quad (8)$$

where γ is the sheath transmission coefficient (γ ~8) and E_H is the ionization energy of hydrogen (13.6 eV), which is deposited at the divertor target when each electron-ion pair recombine. This leads to the divertor heat flux to be minimum at $T_{div} = E_H/\gamma$ (~ 2 eV) under these assumptions and to a maximum reduction of the power flux to the divertor by plasma radiation of not more than a factor of 2 under these assumptions.

In fact, when approaching divertor temperatures under 5 eV other atomic processes dominate the divertor momentum and particle balance [Stangeby 1993, Borrass 1997]. Large momentum losses through the interaction of the ions flowing towards the divertor target and the recycling neutrals take place which slow down the ion flow. In addition, the recombination of electrons and ions in the high density/low temperature divertor plasma conditions causes a significant particle sink at the divertor. These two processes break the link between the main SOL plasma parameters and those at the divertor given by Eqs. 5 and 6 leading to the so-called detached divertor regime. This allows, in theory (i.e. without any consideration of other integration issues), the power outflow from the main plasma to be fully exhausted by radiative and atomic losses at the divertor as shown for a JET density scan in Fig. 5. In addition to the power exhaust solution, achievement of cold divertor conditions and detachment also leads to conditions with very low sputtering of W so that in this case the power exhaust solution and the minimization of W impurity sources result of the same divertor physics regime. This regime is the so-called detached divertor regime which has been reproduced in all divertor tokamaks [LaBombard 1995, Loarte 1998, Wenzel 1999, Petrie 1997] and its basic ingredients confirmed. It should be noted, however, that the quantitative identification of the atomic processes that lead to the momentum and particle losses and of the processes dominating the radiative losses in present experiments and which of them will be relevant for ITER and DEMO burning plasmas remains the subject of R&D [Kukushkin 2009, Wischmeier 2015].

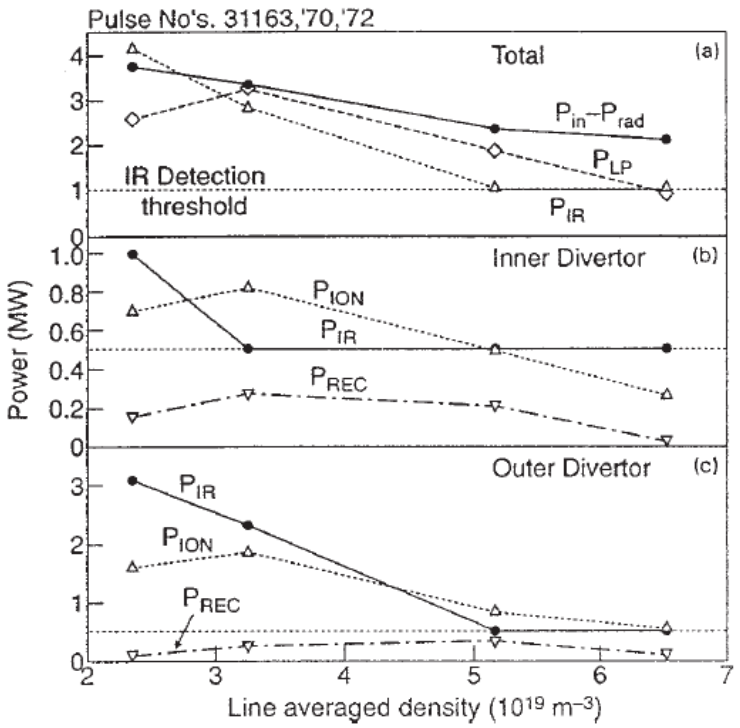

Figure 5. Power deposited at the divertor target for range of JET experiments as determined from the input power and plasma radiation, from infrared thermography (PIR) and derived from Langmuir probes ($P_{LP} = P_{ION}+P_{REC}$), where P_{ION} is the power deposited by deuterium

ions and electrons while P_{REC} is the power associated to the recombination of each electron-ion pair. a) shows the total power balance while b) and c) show measurements at the inner and outer divertor. P_{REC} is found to decrease at high densities with the onset of plasma detachment [Loarte 1998].

Plasma detachment is generally observed to start at the strike point and then to proceed further outwards in the divertor plasma. This leads to a decrease of the particle and power flux near the separatrix (partial detachment) that then proceeds outwards in the SOL until the power and particle flux to the target vanish achieving the so called total detachment. With the increase of the degree of plasma detachment the ionization/recombination front and divertor plasma radiation move away from the divertor towards the X-point. In the final states of the process a significant fraction of the plasma radiation can come from inside the plasma separatrix and this can lead to a radiative collapse of the plasma and to a disruption, as shown in Fig. 6.

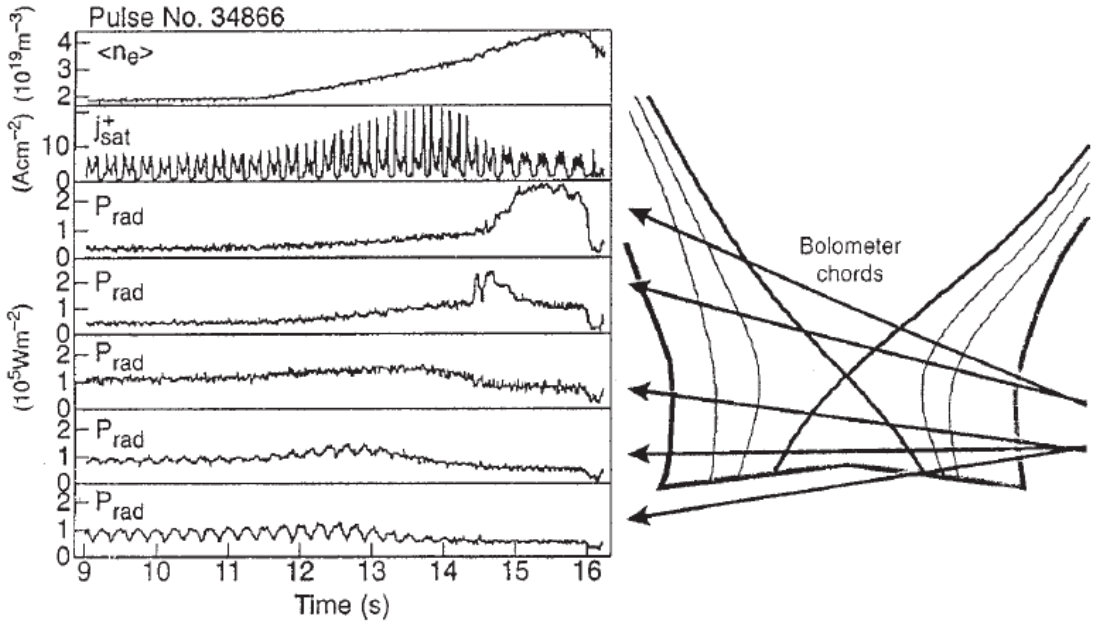

Figure 6. Evolution of the measured radiation along various chords within the JET divertor showing the radiation migration towards the X-point as the divertor ion flux decreases with the onset of detachment (top row) [Loarte 1998].

The degree of plasma detachment can be actively controlled to some degree through gas fuelling, extrinsic impurity seeding and through the additional heating level [Monk 1996, Mertens 2000]. The sensors used for this control that have been typically used in experiments include the ion flux [Guillemaut 2007], the thermoelectric current flowing between the inner and outer divertor (which depends on electron temperature at the divertor) [Kallenbach 2015] and the local radiation at the divertor [Giroud 2013]. The degree of detachment control that can be achieved varies with plasma conditions, level of extrinsic impurity species, etc. and it is intrinsically influenced by the thermal stability of the radiation and ionization front at the divertor, i.e. how stable the radiation and recombination/ionization balance is in the divertor under small perturbations that lead the plasma to attach or the radiation to accumulate at the X-point and to penetrate inside the confined plasma.

The geometry of the divertor has been found to affect the access to divertor detachment and the associated strong reduction of divertor power fluxes due to its direct effect on the neutral recycling flux. Plasma ions are neutralized at the divertor target and then re-emitted into the plasma in a direction perpendicular to the target, on average. Depending on the relative angle between the divertor target and the magnetic field line this can increase the plasma density near the separatrix or away from it. The modification in neutral recycling pattern caused by the divertor geometry can affect the favourable approach to total detachment of the divertor described above (i.e. reduction of the power flux largest near the separatrix where the power flux has its maximum value before detachment starts). For instance, detachment can start away from the separatrix and then proceed towards with inclined horizontal divertor targets, as seen as JET shown in Fig. 7 [Monk 1997]. It should be noted, however, that the magnitude of these divertor geometry effects on detachment is also strongly influenced by the divertor plasma parameters themselves (neutral ionization mean-free path) and neutral parameters (neutral-neutral mean free-paths). As the ratios of these mean free paths with respect to the spatial dimensions of the divertor plasma becomes smaller, the physical processes that determine plasma detachment become more localized and the global effects from divertor geometry associated with changes in recycling pattern and non-local neutral effects decrease in magnitude. An example of this, is for instance, the effect of neutral baffling near the corner of a vertical divertor target, which causes strong the modifications to detachment access in JET in Fig. 7 but is modelled to have minor effects in ITER where the neutral-neutral mean free path is small compared to the divertor plasma dimensions [Kukushkin 2005]. Similarly, the behaviour of hydrogenic radiation is expected to be different in ITER and DEMO than in most of present experiments as neutral densities become large enough for the radiation emitted by hydrogenic atoms to be trapped by other atoms in the divertor. This phenomenon has been identified in present experiments at high density such as Alcator C-Mod [Lisgo 2005] and modelled to affect plasma parameters at the ITER divertor [Kukushkin 2005] but not in a sufficient large way as to change the divertor properties significantly. However, it remains to be seen if this behaviour can actually finally affect the maximum radiation fraction that can be achieved both in conventional and advanced divertors for DEMO-like plasmas.

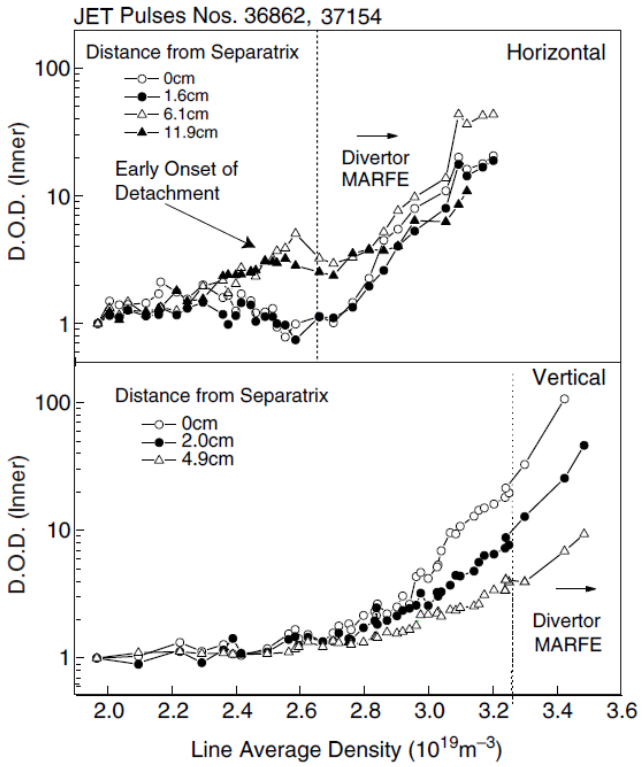

Figure 7. Degree of detachment for the inner divertor at various distances from the separatrix for two JET-MkIIA density scans. The upper figure the early onset of divertor detachment starting away from the separatrix in horizontal divertor discharges while the lower figure shows the more conventional behaviour of detachment starting near the separatrix and proceeding further outwards in the SOL for a vertical divertor configuration [Monk 1997].

A key issue regarding power exhaust for ITER and DEMO is the level of plasma radiation and/or the decrease of the power flux from that in attached conditions that can be achieved at the divertor while most of the radiated power is confined in the divertor channel itself (not concentrated at the X-point) and thus not affecting the confined plasma. Present experimental results and modelling predictions for ITER indicate that a reduction of the heat flux down to 10 MWm^{-2} for ITER Q=10 operation can be achieved in partial detached divertor operation with ~ 70% of the power crossing the separatrix being radiated at the divertor [Pitts 2013]. Increasing the degree of plasma detachment beyond this level leads to the radiation concentrating at the X-point and to total detachment at the divertor target. While the partially detached regime in the conventional divertor is expected to be sufficient to achieve ITER's goals, it is not appropriate for DEMO if the level of radiation in the core plasma is maintained at a similar level as ITER (i.e. $P_{rad}^{core} \leq$ 30-40% P_{tot}, where P_{tot} is the total plasma heating power). For DEMO P_{tot} is expected to be at least 3-4 times larger than in ITER while the power handling engineering limit of the PFCs is expected to remain roughly the same (~10 MWm^{-2}). This requires that ~ 90% of the power crossing the separatrix is radiated at the divertor. This is not presently achievable in conventional divertors, i.e. with similar design to that of ITER, while avoiding the radiation to migrate to the X-point and with strong effects on the energy confinement of the plasma and/or plasma disruptions.

To increase the maximum divertor radiated power level and to reduce the power flux at the target beyond that achieved by the conventional vertical divertor, the advanced divertor geometries described in section 2 have been proposed. These divertor geometries aim:

a) to increase the effective volume of the divertor by modifying the poloidal flux expansion in the divertor volume itself and/or locally near the divertor target (snowflake, X-divertor and super-X), and,

b) to improve the thermal stability of the divertor plasma at high radiative fractions by modifying the variation of poloidal flux expansion between the divertor and the X-point compared to the conventional quadrupole X-point (X-divertor and super-X).

In addition to this, the snowflake configuration is expected to further increase the divertor radiated power level by increasing anomalous transport locally in the divertor region itself through the effect of the extended region with low poloidal field around the X-point(s) [Reimerdes 2013]. The super-X divertor, on the other hand, aims to reduce the magnitude of the power flux along the field by toroidal flux expansion and diffusion into the private flux region so that the magnitude of the plasma power flux density that needs to be dissipated by plasma radiation is smaller than that in a conventional divertor. The detailed description of these configurations and their expected effects on detachment, radiation and divertor power fluxes and initial experimental results is beyond the scope of this paper and can be found in accompanying papers in this special issue.

Open issues that affect both conventional and advanced divertors are: to which level the limits in achievable power flux reduction by divertor radiation are determined by the divertor detachment level and the stability of the solution against changes in the edge plasma transport when the divertor plasma becomes dense and cold. In experiments, it is frequently observed that, with the establishment of dense/cold divertor conditions with high radiative losses, anomalous transport in the SOL increases and, together with this, the power fluxes to main chamber PFCs increase in detriment of the divertor. Two physics pictures are put forward to explain this behaviour: a) the increase of divertor radiated power and the movement of maximum radiation emission towards the X-point lead to an increase of anomalous transport at the plasma edge associated with the decrease of power outflux from the main plasma [Loarte 1998]; this eventually leads to the increase of power fluxes to the main chamber PFCs and to a decrease of the divertor power fluxes which can eventually lead to the thermal collapse of the plasma or b) the formation of a high density/low temperature plasma at the divertor and/or plasma detachment affects the relation between transport along the field and across the field (transport along the field damps turbulent transport across the field) as the radial structures produced by turbulent transport in the SOL become “disconnected” from the divertor target [Carralero 2015], as shown in Fig. 8 for the density profiles; this increased particle transport can potentially increase the power fluxes to the main chamber PFCs which reduces the divertor power flux and affects the level and location of plasma radiation within the divertor volume. Depending on which of these two possible mechanisms contribute to the ultimate level of divertor radiation that can be achieved in high confinement regimes, the possible advantages of each of the advanced divertor configurations with respect to the conventional divertor in increasing this level will be quantitatively different.

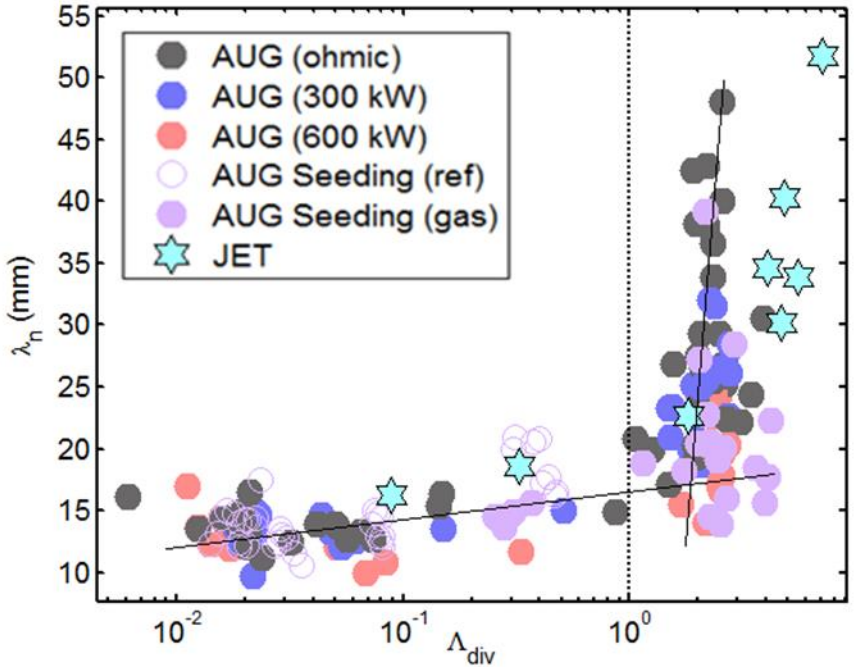

Figure 8. SOL density scale length versus the divertor plasma effective collisionality parameter (for $\Lambda_{div} > 1$ the SOL plasma turbulent plasma structures are disconnected from the divertor targets) [Carralero 2015].

4. Power dissipation by radiation in the confined plasma and core-edge compatibility issues

In addition to dissipation of power by atomic and impurity losses at the divertor, it is also possible to decrease the power that flows to the divertor target PFCs by increased core plasma radiation. Obviously, such increase must be compatible with maintaining the required plasma performance for high gain fusion power production. This involves both maintaining an appropriate edge power flow to sustain high quality H-mode confinement and a sufficiently low central impurity concentration to ensure that fuel dilution and radiative losses from the central plasma region where fusion reactions take place are kept limited. These compatibility issues affect quantitatively the contribution of core radiation to the solution of the power exhaust problem depending on the plasma parameters and edge power flow. This scheme is not expected to be a major contributor to the power exhaust issue in ITER high Q regimes while it is essential to the conventional divertor approach to DEMO. Core plasma radiative power exhaust could also contribute to the advanced divertor approaches if limitations are found in the achievable divertor radiation at levels lower (< 90%) than those required for DEMO operating with low core radiative fraction.

Sustaining the high confinement regime required for fusion reactors requires the edge power flow to exceed a given threshold. This threshold is empirically found to depend on plasma surface, density and toroidal field [Martin 2008] and when it is exceeded a transport barrier at the edge is formed and the H-mode regime is accessed. Achievement of high energy confinement usually requires that the edge power flow remains by an appropriate margin above this threshold value (typically at least 15-30%) [Martin 2008, ITER Physics Basis 2007]. This prescription has been shown to also describe well experiments with varying levels of core radiation from extrinsic experiments such as in Alcator C-Mod [Hughes 2011], as shown in Fig. 9, although other edge plasma effects also play a role on the achieved energy confinement in these conditions, as discussed later in this section.

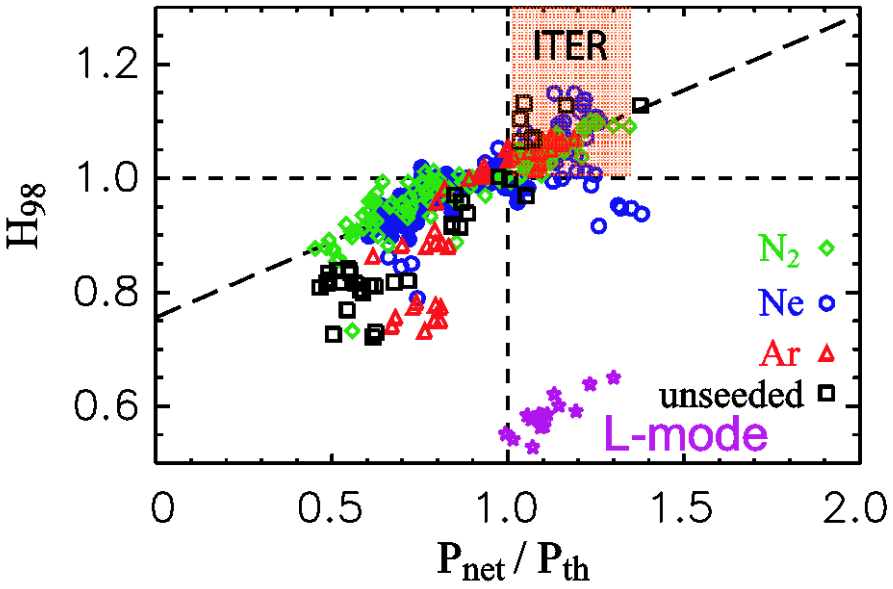

Figure 9. Normalised energy confinement versus net power crossing the separatrix (P_{net}) normalized to the H-mode threshold power (P_{th}) for EDA H-modes in Alcator C-Mod with extrinsic impurity seeding (N_2, Ne, Ar) and with intrinsic impurities (unseeded). The normalised energy confinement in L-mode discharges is shown for comparison [Hughes 2011].

Given the expected value of the H-mode threshold in ITER and DEMO from [Martin 2008], and assuming a margin of 25% above this value to sustain good H-mode confinement, the maximum level of core radiation that can be sustained in the two devices (in relation to the total plasma heating power) is significantly different, as shown in Table 1.

Device	P_{tot} (MW)	P_{L-H} (MW)	P_{sep}^{min} (MW)	$P_{rad}^{core,max}$ (MW)	$P_{rad}^{core,max}/P_{tot}$ (%)
ITER (Q=10)	150	70	88	62	41
DEMO	460	133	166	294	64

Table 1. Total heating power (P_{tot}), H-mode threshold power (P_{L-H}), minimum edge power flow compatible with high confinement assuming a margin of 25% above P_{L-H} (P_{sep}^{min}) and corresponding maximum radiated power in the plasma core ($P_{rad}^{core,max}$).

Indeed DEMO-like solutions with strong core plasma radiation to the power exhaust problem have been demonstrated in present experiments such as in the ASDEX-Upgrade example shown in Fig. 10 [Kallenbach 2013], where Krypton is used to increase core radiation while Nitrogen is used to increase divertor radiation with reduces the divertor power fluxes to very low values while the plasma remains in the high confinement regime. If these levels of core radiation can be achieved in a compatible way with high fusion performance and adequately controlled in DEMO then the overall solution to divertor power exhaust of the remaining power flowing out of the confined plasma would not be significantly different between DEMO and ITER.

In this respect, it is important to note that the specific features of the core and pedestal plasma in ITER and DEMO can make this goal simpler to achieve than in present experiments. Indeed the low level of neutrals escaping from the divertor and the associated low particle

source from recycling neutrals is predicted to lead to relatively flat density profiles in the edge transport barrier, as shown in Fig. 11 for ITER gas fuelled H-modes [Romanelli 2015]. In these conditions the density gradient at the plasma edge can be controlled by the core particle source provided by pellets. These shallow edge density gradients at the plasma edge make the transport of impurities from the separatrix into the core plasma very inefficient due to the large screening provided by the temperature gradient in the edge transport barrier, where impurity transport is found to be well described by neoclassical physics in the experiment. This allows significant impurity density gradients to be sustained in the ETB as shown in Fig. 12 [Dux 2014] for ITER where the density inside the edge transport barrier can be easily be up to 100 times lower than at the separatrix for the case of W impurities.

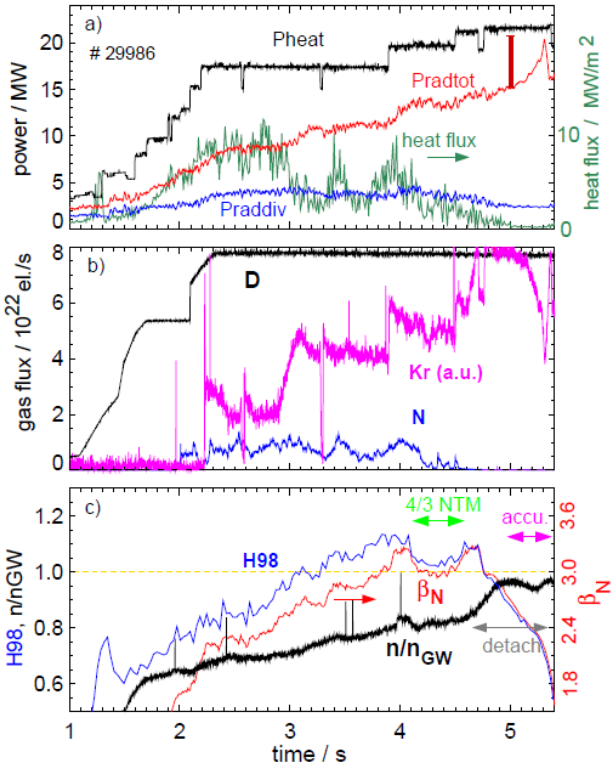

Figure 10. Time traces for an ASDEX-Upgrade discharge which combines N and Kr seeding where core radiation is increased to its limit by Kr injection [Kallenbach 2013].

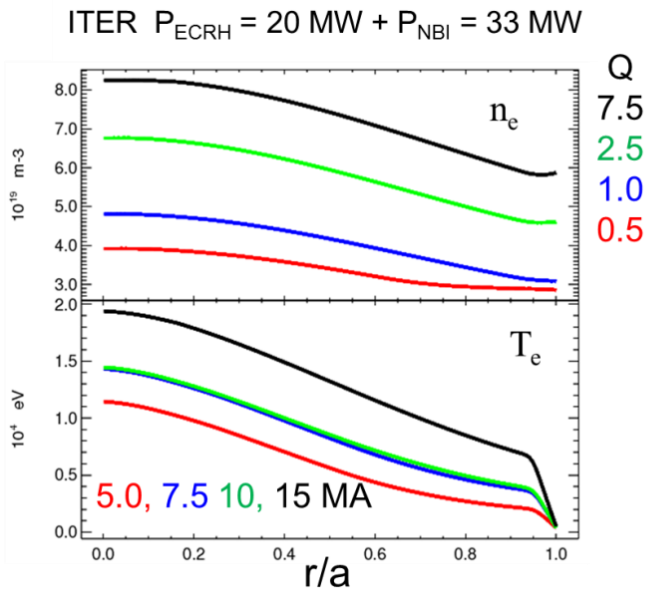

Figure 11. Radial profiles of the plasma density and temperature in ITER DT gas fuelled H-mode plasmas for a range of plasma currents showing flat density profiles at the plasma edge (r/a = 0.95-1.0) in the pedestal transport barrier with steep temperature profiles [Romanelli 2015].

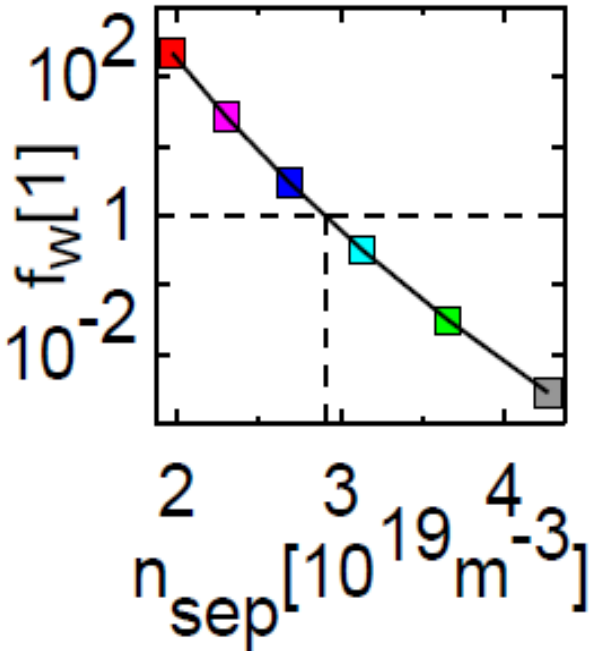

Figure 12. Ratio of W density inside the edge transport barrier to the separatrix versus electron separatrix density for ITER Q =10 plasma conditions. For separatrix densities larger than $3 \cdot 10^{19}$ m^{-3} the W density inside the edge transport barrier can be significantly smaller than at the separatrix [Dux 2014a].

Given that the extent of the edge transport barrier is typically ~ 3% of the plasma minor radius and the fact that the volume of the plasma is largest for the outer shells, the plasma volume in which these large impurity densities can be sustained is relatively large (V_{edge} ~ 250 m^3 in DEMO, i.e. 6% of the total plasma volume), the potential to provide significant

power exhaust from this edge layer is very large. The total radiation that can be emitted from the edge layer is thus given by

$$P_{rad}^{edge} = V_{edge} \text{ x } n_{edge} \text{ x } C_{edge} \text{ x } L(T_{edge}) \quad (9)$$

Where n_{edge} is the average plasma density at the pedestal in DEMO (~ 5 10^{19} m^{-3}), $L(T_{edge})$ the temperature averaged radiation efficiency for the impurity considered and $C_{edge} = n_{Z,edge}/n_{edge}$ the average impurity density concentration. For instance, Ar has a radiation efficiency of 1-4 10^{-33} Wm^3 for T_e in the range 1-10 keV, typical of the plasma pedestal in DEMO, and a core impurity concentration lower than 1% is required to have acceptable fusion performance in DEMO (dilution < 15% decreasing fusion power < 30%) . In this case if C_{edge} can be sustained at a level typically one order of magnitude larger than in the core, then P_{rad}^{edge} ~ 100's MW. It should be pointed out that according to pedestal neoclassical transport the peaking of the impurity density at the plasma edge provided by temperature screening scales as [Dux 2014a]

$$n_Z^{core}/n_Z^{sep} \sim e^{<Z>} \quad (10)$$

where <Z> is the average charge of the impurity in the edge region. For the case of Ar this is 17-18 for typical ITER and DEMO conditions while for W is 35 [Dux 2014a]. Therefore, the increase of W density from the pedestal to separatrix by a factor of 100 as predicted for ITER and DEMO plasma conditions corresponds to a factor of 25 for Ar thus making the core radiative solutions for DEMO rather feasible. In fact such core radiative solutions with acceptable plasma performance have been obtained for DEMO on the basis of the ASDEX-Upgrade experiments for Kr and Ar, as shown in Fig. 13, even without taking advantage of the increased edge impurity concentrations provided by the strong temperature screening described above. The radiation emitted from the core plasma is expected to be rather poloidally symmetric due to the low normalized toroidal rotation speed expected in ITER and DEMO plasmas so that the resulting power loads on the first wall due to core radiation are rather moderate ~ 0.2 MWm^{-2}.

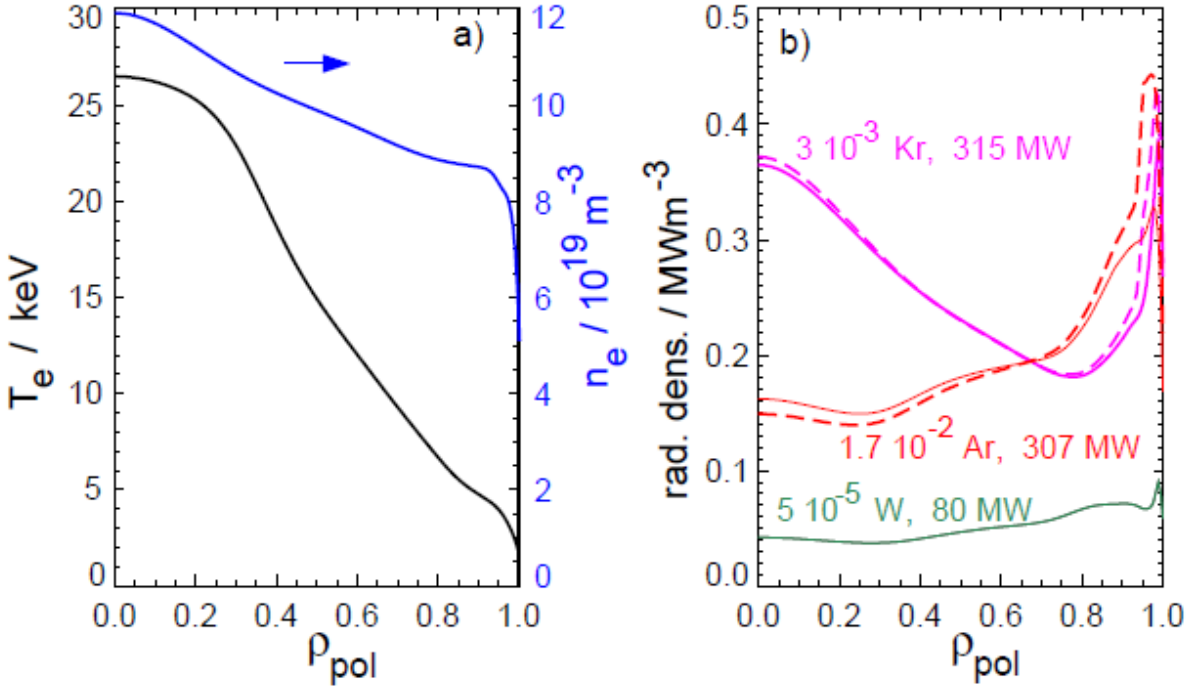

Figure 13. a) DEMO plasma profiles and b) radiation profiles for Ar, Kr and with concentrations c_Z constant across the radius and corresponding radiated powers in the plasma [Kallenbach 2013].

An important open issue regarding edge impurity screening is to which level the pedestal profiles which are favourable to provide high edge radiative conditions are compatible with high fusion performance, specifically the high separatrix densities which are required for divertor power load dissipation especially for low values of lambda-q as shown in Fig. 14, compared to the optimum values of the pedestal and core densities for fusion performance.

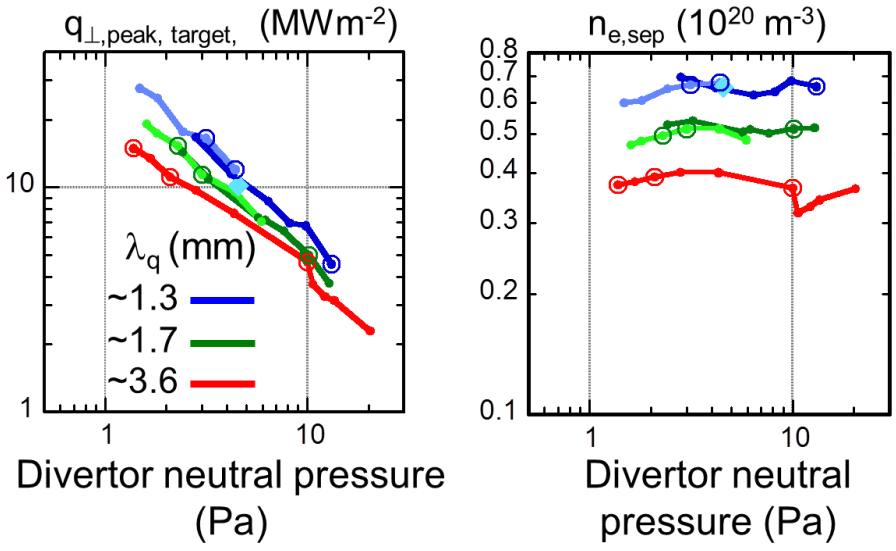

Figure 14. Predicted ITER peak divertor power flux and associated separatrix density versus divertor neutral pressure for a range of anomalous transport assumptions leading to various λ_q [Kukushkin 2013].

Increasing separatrix densities is found in present experiments to degrade H-mode plasma performance but the physics of this process is not yet fully understood. Recent analysis of experimental results indicate that the reduction of performance is due to changes in the magnitude and location of the ionization source from recycling neutrals that affect edge MHD stability and reduce the maximum achievable pressure [Dunne 2017]. Modelling studies indicate that, on the other hand, plasma transport in the pedestal could be increased for such density profiles thus decreasing energy confinement [Hatch 2017]. Depending on which of these two possible mechanisms is dominant, the consequences for ITER and DEMO regarding the achievable edge impurity densities (through the effect of temperature screening) with good confinement will vary. In particular, neutral source driven effects are not expected to play a major role in ITER and DEMO and thus no significant reduction of edge MHD stability is expected due to effects associated with edge ionization. Ultimately, the possible restriction of the range of separatrix densities achievable with high confinement H-modes could be the limiting factor to the achievable level of core radiation in DEMO. In this respect, it is possible that advanced divertor configurations, which potentially allow operation with lower separatrix densities for a given level of edge power flux compared to the conventional divertor, may also offer a wider operational range of plasma conditions in which high core radiative fractions can be made compatible with high fusion production plasmas.

Obviously, such an edge radiative solution depends on up to which degree the resulting core impurity concentration is compatible with fusion performance. In this respect the compromise results from the balance of the dilution of DT fuel and increased radiation losses in the core plasma. For medium-Z impurities, such as Ar, the effect of dilution is larger because these impurities are fully ionized in the core plasma and only cause bremsstrahlung losses. For higher Z impurities, such as Kr, radiation losses are more important because these species are not fully ionized in the core, as shown in Fig. 13.b. An additional important issue is that core impurity transport can be unfavourable and lead to accumulation of impurities in the plasma core, which is driven by neoclassical transport impurity transport, as sometimes found in experiments with high Z PFCs. Such accumulation would lead to the strong reduction of the fusion performance and most likely to a plasma disruption if it were to occur in DEMO. In this respect, it is important to note that the situation regarding core impurity accumulation is predicted to be much more favourable in next step than in present devices. This is an essential ingredient for the viability of the high core radiative approach to power exhaust in DEMO. The two key differences identified that make the situation more favourable for next step plasmas are indeed intrinsic to reactor plasmas and these are: a) the lack of a sizeable source of particles in the core and b) the dominance of electron heating. The former affects the central plasma density peaking which is then solely determined by transport physics and predicted to be very moderate in ITER and DEMO [Loarte 2015b], while the latter affects the nature of core impurity transport itself that can deviate strongly from neoclassical transport when electron heating is dominant [Angioni 2017a]. The consequence of the two effects is that no or very moderate core impurity accumulation is expected in ITER and DEMO, as shown in Fig. 15 for W in ITER. It is important to note that these predictions have been confirmed by experiments: the central particle source provided by NBI source has been found to be required to explain the observed D peaking and the ensuing W accumulation at JET [Angioni 2014, Mantica 2013] while the role of electron heating in determining the observed W peaking has been quantitatively demonstrated in ASDEX-Upgrade experiments, as shown in Fig. 16 [Angioni 2017b].

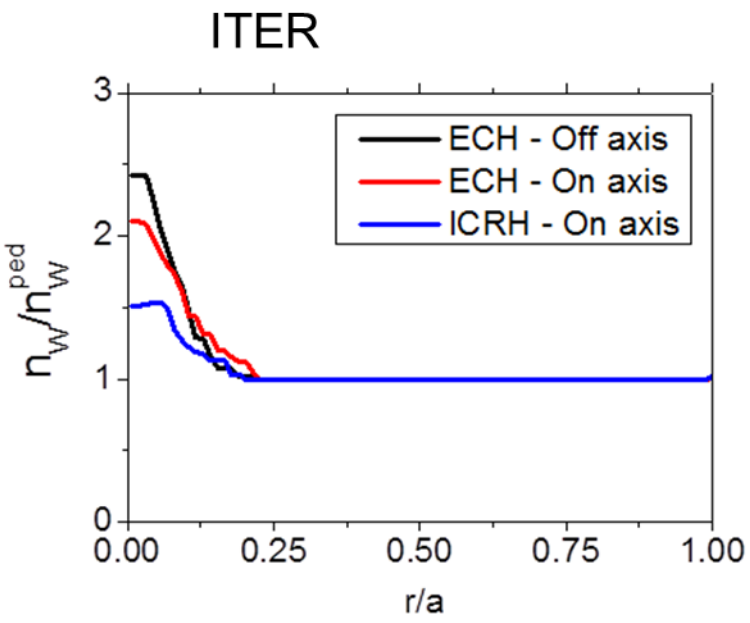

Figure 15. Modelled W density profiles in ITER Q = 10 plasma with 33MW of NBI and 20 MW of ECH or ICH heating, showing very moderate impurity accumulation in the plasma centre [Loarte 2015b].

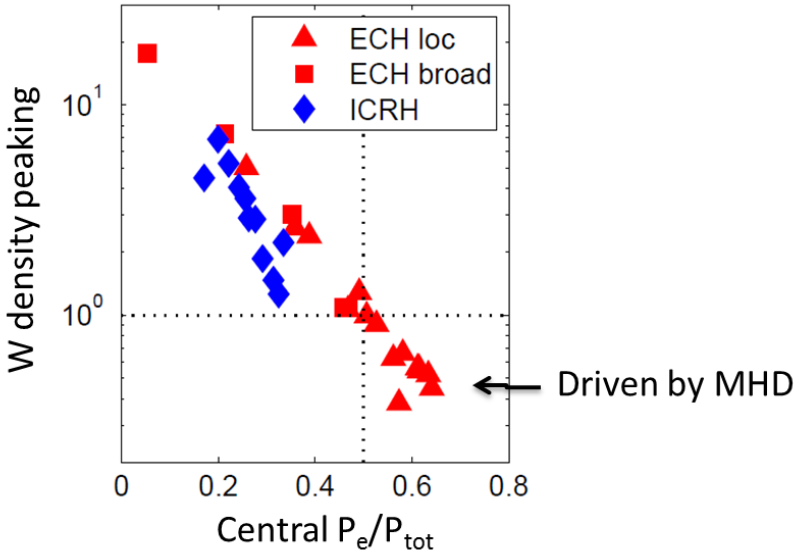

Figure 16. Measured W density peaking versus central electron power in H-mode experiments in ASDEX-Upgrade with ECH and ICH heating [Angioni 2017b].

5. Power exhaust during confinement transients and ELMs

In addition to the exhaust of power during stationary phases discussed above, power exhaust must also be provided during transients that take place during H-mode scenarios in energy confinement time timescales (transitions between L-mode and H-mode regimes) and MHD timescales (ELMs) and/or avoiding such fast transients.

Providing power exhaust during H-mode access and exit is not conceptually different from stationary H-mode conditions. However, it is much more complex due to the inter-relation between the actuators that are required to provide exhaust and the evolution of the energy confinement in the plasma itself, as the access/sustainment of the H-mode regime depends on edge power flow levels, plasma density, etc. This is particularly complex for ITER and DEMO because alpha heating is the major contributor to the edge power flow level and this is itself determined by the energy confinement in the plasma whose quality is in turn determined by the edge power flow level. From the two confinement transients considered, the H-mode exit is the most challenging one from the power exhaust point of view, as the plasma energy decreases in this phase leading to increased edge power flows. On the contrary, for the H-mode access phase the plasma energy increases as a result of the increased energy confinement and this leads to relatively low edge power flux levels (marginally above the L-H transition power threshold) compared to those in stationary H-mode conditions. In the H-mode access case the main issue is to ensure that burning plasma conditions can be achieved that are compatible with edge power flux control. ITER simulations have shown that this depends critically on the control of the density after the L-H transition. A too fast rise of the plasma density leads to a colder core plasma with lower fusion energy production and to a higher requirement for the edge power flow to sustain the H-mode, which finally prevent the plasma to reach stationary conditions. In the case of ITER such control can be achieved by the appropriate application of gas fuelling (for separatrix density control) and pellet fuelling (for core density control). Fig. 17 [Koechl 2016] shows the operational space in terms of parameters characterizing density evolution that ensure access to burning plasma conditions with controlled divertor power fluxes and Fig. 18 [Militello-Asp 2016] shows two examples of the modelling core plasma parameter and divertor power flow evolution for two density waveforms one inside and one outside the range to access burning plasma conditions.

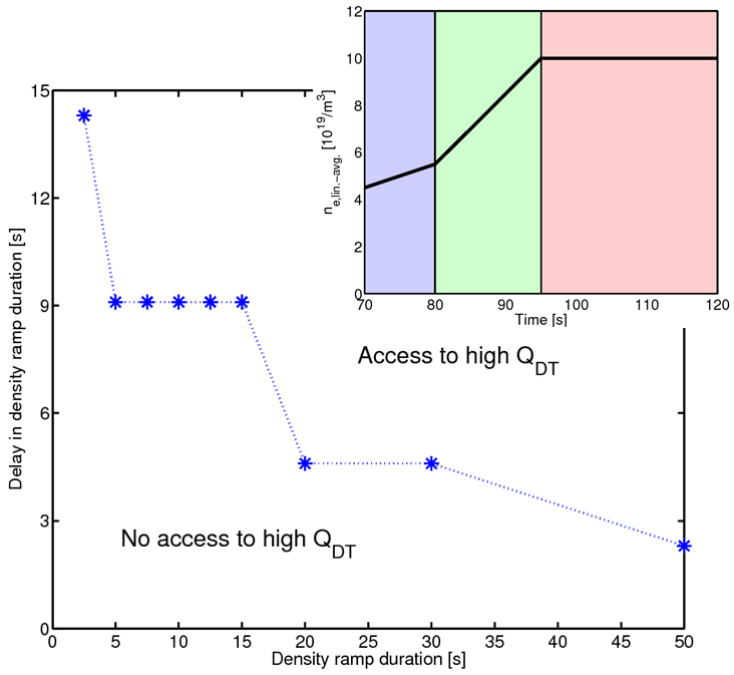

Figure 17. Operational space for the achievement of a transition to high Q_{DT} ~ 10 15MA/5.3T H-mode in ITER for P_{AUX} = 53 MW in terms of the duration of the pellet fuelled ramp to the nominal density (green phase in inset) and of the delay of the ramp in density with respect to the start of the high heating power (blue phase in inset) [Koechl 2016].

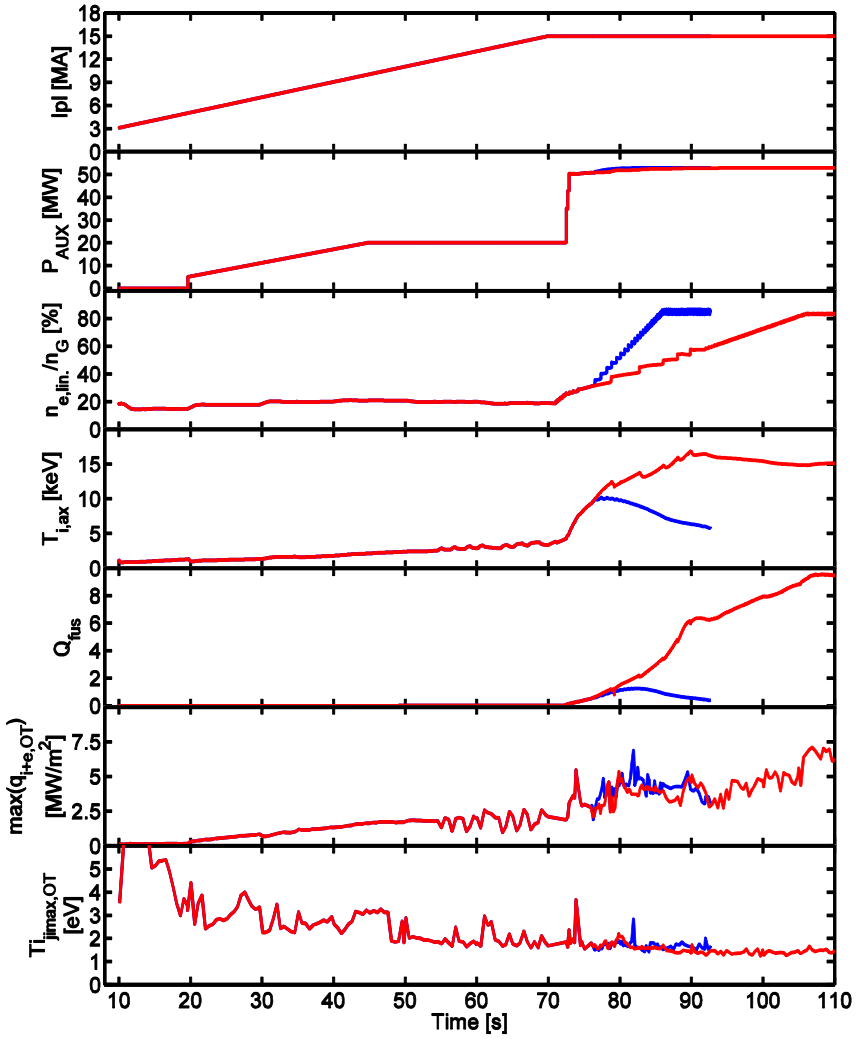

Figure 18. Modelled current-ramp up for ITER DT baseline scenario with L-H transition at 15MA. Slow (red) and fast (blue) pellet density ramp after the transition. From top to bottom: plasma current, additional heating level, line average density, Q and maximum divertor power flux and temperature. The level of 10 MWm^{-2} is not exceeded in the H-mode access phase [Militello-Asp 2016].

As mentioned above, the control of power loads during H-mode termination phase is more challenging. During H-mode terminations the reduction in energy confinement can potentially increase the level of edge power flow significantly above that in stationary H-mode conditions. Initial evaluations for ITER indicated that this increase could be as high as a factors of 2-3 [Loarte 2008]. Later studies of the H-L phase in JET ITER-like experiments showed that this projected high transient power flows are not found in practice due to the inter-relation between the edge power flow level and the sustainment of the H-mode confinement in the H-mode collapse phase, as shown Fig. 19. Indeed the decrease of energy confinement in the H-mode termination phase is a self-regulated process that maintains the edge power flow marginally above the H-L transition level and thus at a value not much higher than during the H-mode stationary phase. Again in this case the main complexity comes from the control of the power fluxes with varying edge plasma and divertor conditions as the plasma energy and plasma density decrease in the H-L transition. Fig. 20 shows an

example or ITER modelling demonstrating that this control is in principle possible. In this case the key issue is to increase impurity seeding, gas fuelling at the divertor and additional heating power to ensure that divertor power fluxes remain low in the initial phase of the H-mode termination when divertor power fluxes are highest and then to decrease them fast enough to prevent the divertor plasma to become thermally unstable, eventually causing a disruption, when the edge power flow decrease later in the H-mode termination phase as the plasma energy decreases.

In these H-mode access and exit phases not only the plasma energy and edge power flow change significantly but also the edge current level driven by bootstrap due to the changes in pedestal pressure. This may pose specific control issues for configurations that require a careful control of the magnetic field structure near the X-point(s) such as the snowflake as these rapid changes in edge current profile can modify significantly the magnetic configuration of the divertor.

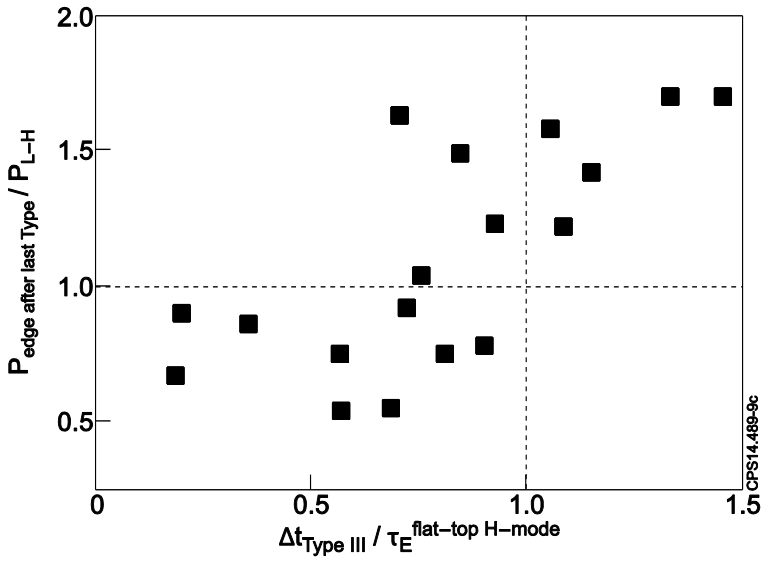

Figure 19. Normalized (to the H-mode power threshold) edge power flow in the Type I ELM H-mode termination normalized (to $\tau_E^{H\text{-mode flat-top}}$) duration of the H-mode termination phase (Type III ELMy H-mode phase) in JET experiments. The horizontal dashed line indicates the points for which the edge power flow is equal to the H-mode threshold power. Similarly the vertical dashed line indicates the points for which the duration of the termination phase equals the energy confinement of the high performance H-mode phase. Larger edge power flow margins above the H-mode transition lead to longer H-mode terminations and thus to a slower decrease of the plasma energy in this phase [Loarte 2014a].

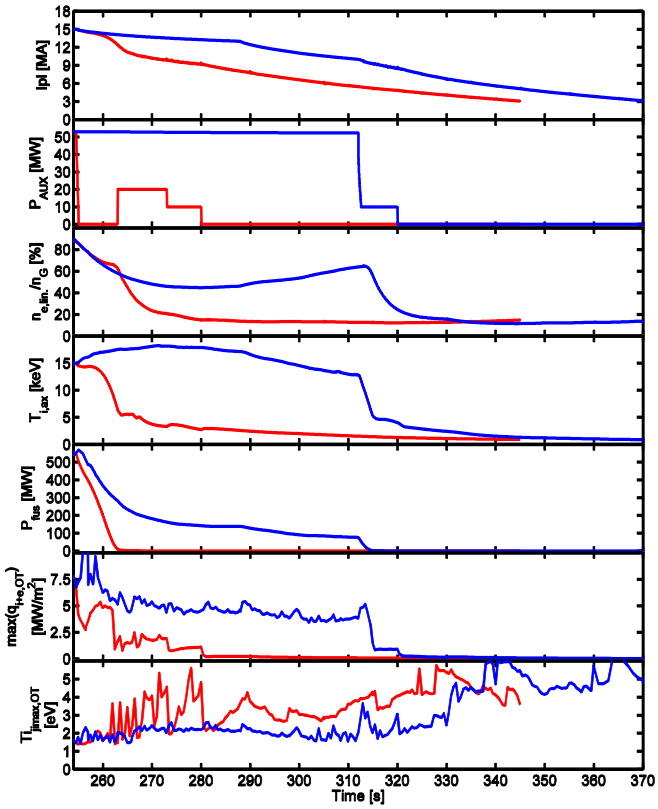

Figure 20. Modelled current-ramp down for ITER DT baseline scenario with H-L transition at 15MA (red) and 10 MA (blue). From top to bottom: plasma current, additional heating level, line average density, fusion power and maximum divertor power flux and temperature. The level of 10 MWm^{-2} is not exceeded in the transition phase from H- to L-mode. The additional heating waveforms in the termination are designed to avoid the divertor plasma becoming fully detached in the termination phase by the impurity seeding and gas fuelling required to control power fluxes in the initial phases of the H-mode termination; this is particularly difficult to control for the at 15 MA due to the larger plasma energy and associated edge power flow levels [Militello 2016].

Control of power fluxes during shorter transients intrinsically associated to high energy confinement and H-mode plasmas, such as ELMs, also needs to be provided. This can be achieved in three possible ways:

a) by operating in a high confinement regime that naturally does not have such transients;
b) by operating in conventional H-mode and by decreasing the transient ELM power fluxes to tolerable levels;
c) by eliminating the ELM transients by active manipulation of the plasma edge stability such as with 3-D magnetic fields applied to the plasma.

A detailed description of all the issues associated with the approaches above is beyond the scope of this paper and the reader is referred to [Lang 2013] for further details. Here we only describe a few specific issues related to power exhaust associated with the ELMs for these three approaches.

- *Operation in high confinement regime without ELMs*

Two candidate confinement regimes to achieve this goal are the QH-mode [Garofalo 2015] and the I-mode [Hubbard]. At present, it is not clear if either regime could be accessible in next step devices such as ITER and DEMO to provide the basis for a high fusion gain scenario and whether any specific divertor design has an effect on them. On the other hand, it appears that for such regimes the schemes for stationary power exhaust are sufficient to provide the solution required.

- *H-mode operation with controlled power fluxes during ELMs*

This approach relies on the increase of the frequency at which these transients are triggered by external means, such as the peripheral injection of pellets, and in this way reducing the magnitude of the resulting power fluxes. The main open issue is whether it is actually possible to decrease the magnitude of the divertor power fluxes or whether just the energy lost during these events is reduced (i.e. the same power fluxes over a smaller area), for which there is contradictory experimental evidence [Baylor 2013, Eich 2017]. When the power densities deposited by ELMs can be reduced significantly, it is found that the divertor plasma can dissipate a significant part of the power flux by transiently enhanced plasma radiation. This was originally modelled for ITER ELMs to occur when the energy loss by ELMs $\Delta W_{ELM} < 1$ MJ and confirmed experimentally at JET [Rapp 2009]. It is important to note, however, that even if this approach could potentially provide a solution for the problem of power exhaust there remain significant open issues related to impurity production and transport and the resulting plasma contamination under such controlled ELMs and to the long term effects of such repetitive loads on the plasma facing materials (cracking, etc.). Physical sputtering of W by ELMs is found to dominate the source of W that can contaminate the confined plasma in present experiments [Dux 2011, Den Harder 2016] and this is also expected to be the case in ITER and DEMO. Even for ELMs that would lead to acceptable divertor transient power fluxes in ITER and DEMO, W sputtering production by ELMs is significant. The influx into the confined plasma of the sputtered W results in radiated power spikes that can be comparable to the total plasma heating power and would cause the termination of the high power phase. The absolute value of these transient W radiation events depends on edge plasma properties, edge W transport (which itself depends on the ELMs) and on the magnitude of the prompt-redeposition of the ELM–produced W which are difficult to evaluate and predict quantitatively [Dux 2014b, Chankin 2014]. Under the assumption that W redeposition is small during the ELMs, it is found that $\Delta W_{ELM} > 1.5$ MJ can produce transient increases of radiation in the main plasma sufficient to cause a loss of the H-mode confinement and fusion power production for ITER Q =10 plasmas, as shown in Fig. 21 [Polevoi 2016]. It should be noted here that this is a worst case estimate because under the conditions expected at the ITER divertor during and after ELMs a significant fraction of the eroded W atoms is expected to be redeposited [Chankin 2014]. In this respect, when evaluating approaches for controlled triggering of ELMs to solve ELM power exhaust issues it is important to also consider W production. In this case, it is not automatically ensured that the solution of the transient power exhaust problem will necessarily provide an integrated solution regarding W production and plasma contamination, contrary to the detached/radiative divertor for stationary conditions in which both solutions are basically provided by the same approach.

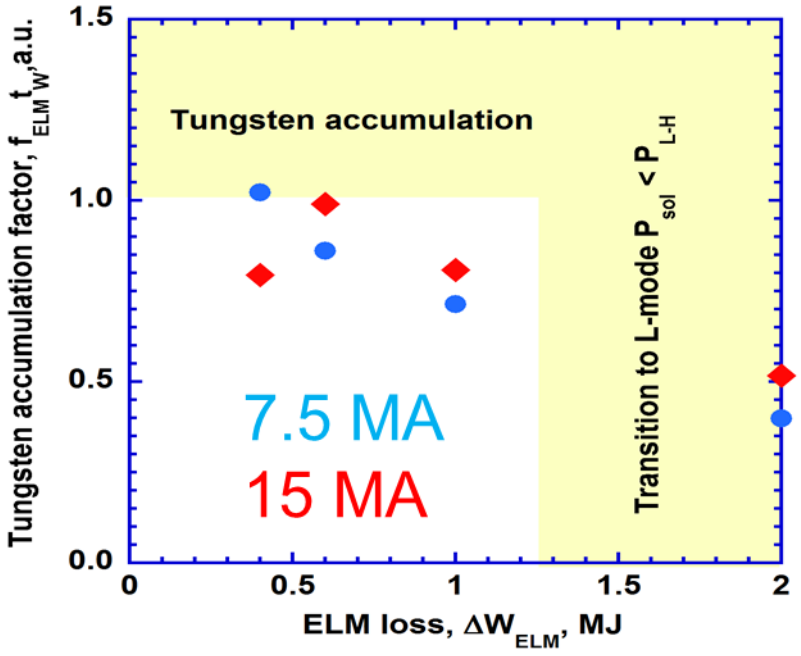

Figure 21. Modelled operational space with good confinement and no W accumulation for ITER DT plasmas at 15 MA/5.3T and 7.5/2.65 T. The vertical boundary at 1.3 MJ is caused by the transient radiation from W produced by the ELM causing an H-L transition due to the ensuing decrease of the edge power flow (no prompt W redeposition during the ELM is assumed) [Polevoi 2016].

- *ELM suppression with 3-D fields*

3-D fields applied to the plasma by magnetic coils can affect edge plasma stability and transport and avoid the triggering of ELMs while the plasma remains in the H-mode regime. The application of these 3-D fields has many effects on the plasma whose description is beyond the scope of this paper, for details of issues considered for ITER the reader is referred to [Loarte 2014b]. Here we specifically concentrate on the power exhaust related issues and in particular to the modification of the magnetic field structure at the plasma edge from toroidally symmetric to asymmetric by the application of these fields. This modification leads to the appearance of a toroidally asymmetric power flux pattern at the divertor with a radial structure made of several peaks, shown in Fig. 22 [Ahn 2014], which correspond to the structure of the poloidal field resulting from the interaction of the externally applied field and the currents that they induce in the plasma itself.

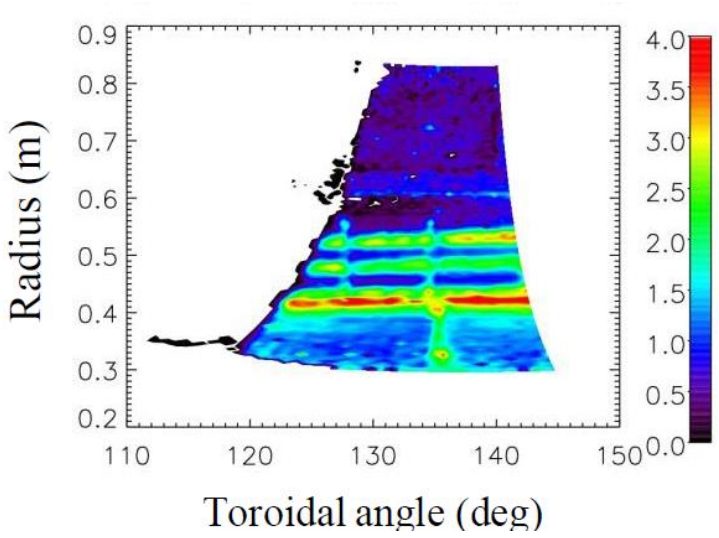

Figure 22. Divertor power fluxes (in MW/m²) following the application of 3-D fields for ELM control in NSTX [Ahn 2014].

This power flux pattern presents specific challenges to power exhaust control, because the local fluxes at a given distance from the separatrix can be much larger than the toroidally averaged fluxes at that location and because it can make the divertor detachment processes to behave in a different way than in the 2-D situation. For instance, the approach to divertor detachment can be potentially affected by the applied 3-D fields with the peak power flux near the separatrix decreasing with increasing density, similar to the 2-D situation, while the peak power flux further away from the separatrix can even increase as shown in Fig. 23 [Ahn 2014, Li 2013].

a) b)

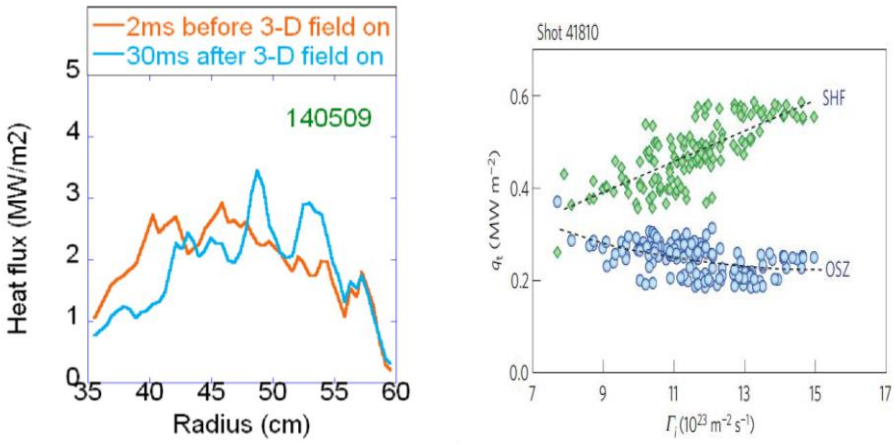

Figure 23. Changes to divertor power fluxes with a 3-D boundary at high plasma densities in a) NSTX versus radius [Ahn 2014] and b) EAST versus divertor ion flux [Li 2013]. With 3-D fields applied significant power fluxes are localised away from the separatrix (SHF in EAST) and they can even increase compared to those at the separatrix as the density/divertor ion flux level increases.

The extrapolation of these 3-D divertor radiative conditions to future devices such as ITER and DEMO remains very uncertain due to both, unknown transport physics and recycling effects, as well as to the prediction of the magnetic structure of the magnetic field itself in

these devices. Initial simulations of ITER plasmas indeed show that the expected local fluxes due to these 3-D field effects can be significant and locally exceed the 10 MWm^{-2} engineering limit, as shown in Fig 24 [Schmitz 2016]. To prevent local overheating of the divertor target, the system of coils that applies the ELM control 3-D fields in ITER will have the capability to rotate the field structure applied at frequencies of few Hz and in this way decrease the time-averaged fluxes at all points of the divertor targets under the engineering limit of 10 MWm^{-2} while avoiding thermal cycling of the divertor PFCs [Loarte 2014b]. While this technique is demonstrated in several tokamak devices (ASDEX-Upgrade, DIII-D, EAST, KSTAR) and a technically feasible approach in ITER, it is foreseen to only apply it when required to ensure appropriate lifetime of these coils, as the number of electromagnetic stress cycles that are applied to these coils is very large for the long pulses considered for ITER.

a)

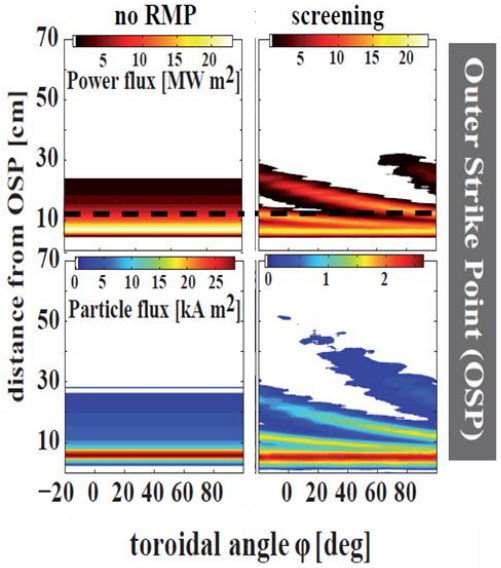

b)

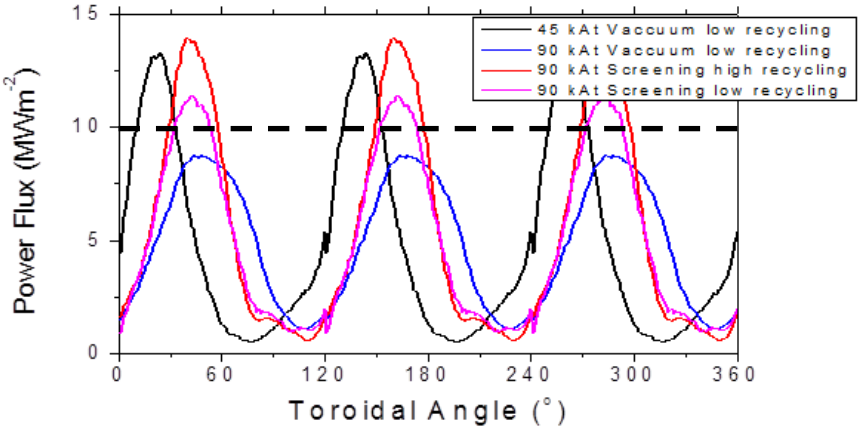

Figure 24. Modelled divertor power and particle fluxes in ITER Q =10 plasmas with and without the inclusion of the effect of 3-D fields applied for ELM control. Significant (> 10 MWm^{-2}) local power fluxes are predicted away from the separatrix at locations for which power fluxes are low in the 2-D situation (dashed line): a) power and particle fluxes at the outer divertor target for a case without 3-D fields and where 90 kAt are applied to the ITER ELM control coils whose field is partially shielded by the plasma, b) power flux profiles

versus toroidal angle for the dashed line in (a)) for 45 or 90 kAt currents in the 3D coils and w/o the effects of plasma shielding on the applied perturbation [Schmitz 2016].

An open issue remains regarding the compatibility of such approach with some of the advanced divertor configurations. The vast majority of the present studies with 3-D fields for ELM control have been performed with conventional divertors and it is not clear how the superimposed edge 3-D field structure will affect the plasma properties at the divertor for some advanced divertor concepts (i.e. snowflake, X-divertor, etc.) and their power exhaust capabilities.

6. Relation between power exhaust and fuel, helium and impurity exhaust

While not explicitly discussed above, the issues related to particle exhaust are strongly correlated with power exhaust. In particular, for a fusion reactor to operate both power and particle exhaust should be appropriate. In many cases the conditions required for power exhaust are well aligned to provide appropriate particle exhaust and impurity exhaust as well. In general, access to high density radiative divertor conditions decreases the ionization mean free path for hydrogen, helium and other impurities and decreases the impurity sputtered source from the divertor. This is accompanied by increased local ionization of hydrogen and impurities at the divertor and to the increase of their neutral densities at the divertor thus allowing efficient pumping of hydrogen and providing impurity exhaust. As mentioned in sections 4 and 5, besides the divertor itself the pedestal plasma and ELMs also play a very important role in providing impurity exhaust from the main plasma and reviewing this topic in detail is beyond the scope of this paper. Here we specifically concentrate on aspects where meeting the power exhaust requirements does not necessarily contribute to providing the required plasma exhaust. One such possible example is helium exhaust; because helium has a higher ionization potential than hydrogen and the other impurities it is ionized further away from the target. This leads to a poorer entrainment of helium in the hydrogenic flow towards the divertor compared to other impurities and to a higher escape fraction as a neutral atom than that of deuterium. As a result, it is frequently observed that the He concentration in gas pumped from the divertor is lower than that in the confined plasma; this is the so-called helium de-enrichment.

Due to these factors He enrichment is found to be worse in many divertor experiments when the conditions for optimum divertor power exhaust are reached, as shown in Fig. 25 for JET Groth 2002] . This has raised the question if there is a real issue between the compatibility of helium exhaust with power exhaust in fusion reactors. Fortunately, whether this is an issue or not depends on divertor plasma parameters, being more favourable for fusion reactors than for present experiments, and on divertor design. The large dimensions of the divertor plasma and the high temperatures and densities expected in ITER and DEMO lead to a very high ionization efficiency of the recycled hydrogenic and helium neutrals in the divertor plasma even when this is partially detached near the divertor target for power flux control [Kukushkin 2009]. On the other hand, exhaust of helium depends on the concentration that can be reached at the pumping plenum and this is determined by whether recycled helium can reach more or less effectively that plenum than DT, which in turn depends on divertor geometry and on the location of the divertor pump. For the conventional vertical divertor configuration with pumping through the private flux region such as ITER, the achievement of satisfactory power exhaust by partial detachment is not only compatible with good helium exhaust but even more plasma detachment is required to achieve it. Divertor detachment is essential to decrease the divertor temperature and density near the separatrix so that the recycled helium can penetrate through the plasma into the private flux region and can be pumped from there, as shown in Fig. 26 [Loarte 2001]. At present systematic studies or

experiments assessing this specific issue have not yet been carried out for most of the advanced divertor geometries in relevant plasmas for DEMO. In view of future research in this area towards DEMO, it is important that all the possible approaches investigated to provide power exhaust also take into account this compatibility issue with helium exhaust to make sure that a self-consistent solution to power and helium exhaust is provided by the most promising advanced divertor configurations explored (i.e. including a suitable geometry for divertor pumping).

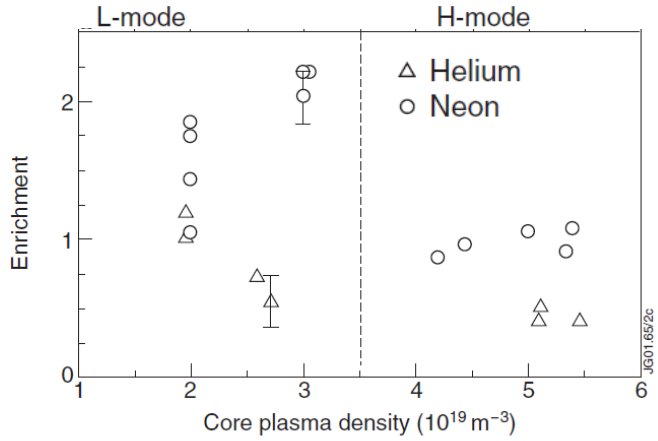

Figure 25. Measured enrichment factors for helium and neon in JET with the MkIIGB divertor for L-mode and ELMy H-mode plasmas. With increasing density and onset of detachment in L-mode the helium enrichment decreases while the neon enrichment increases. In attached ELMy H-mode conditions He enrichment is lower than in L-mode [Groth 2002].

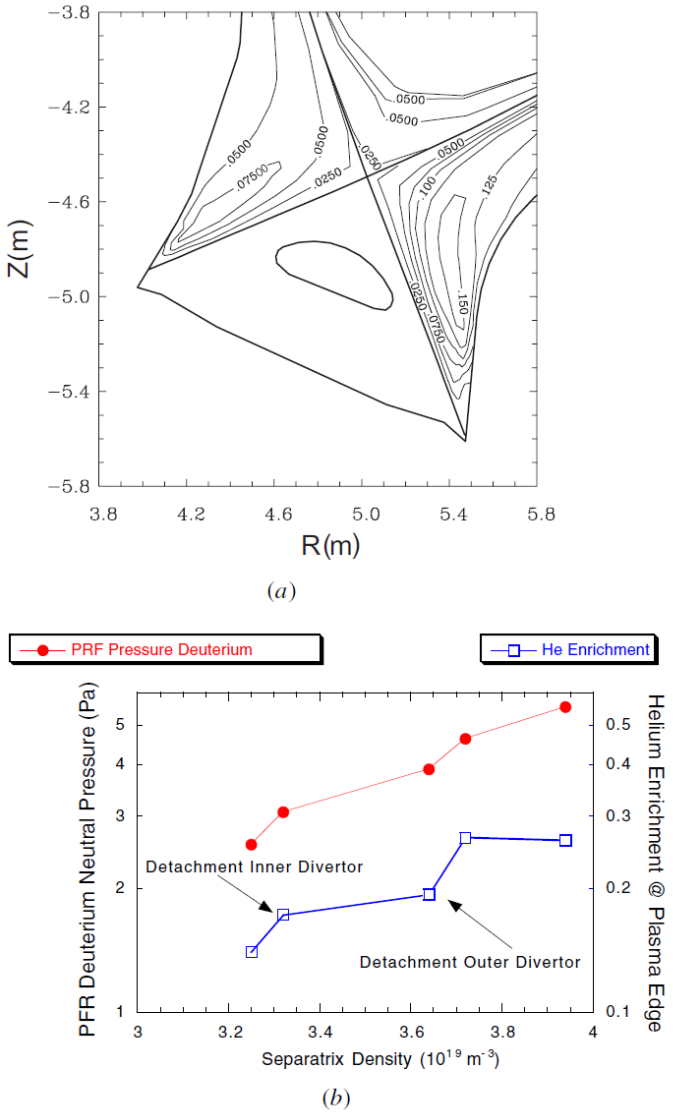

Figure 26. a) SOLPS modelled contours of the He concentration (n_{He}/n_e) in the ITER divertor showing a clear peaking away from the separatrix, which is typical for He. b) SOLPS modelled DT pressure and helium in the ITER PFR versus the separatrix density. A stepwise increase in He enrichment is obtained when the inner and the outer divertor reach divertor detachment. Pumping of DT and He is performed in ITER through the divertor private flux region [Loarte 2000].

5. Conclusions

The solution of the power exhaust problem remains a key open issue for the demonstration of fusion reactors based in the tokamak concept. Besides the use of alternative divertor target designs with the use of liquid metals, two main approaches are presently being considered one based on the conventional divertor approach and the other on advanced divertors. The conventional divertor follows the ITER power exhaust strategy based of partially detached divertor operation supplemented by a significantly increased core radiation level to reduce the edge power flow in DEMO to similar levels to those in ITER. This is a viable option in DEMO unlike ITER because the larger total heating power due to the large fusion production and associated larger margin over the H-mode threshold power. The main open question for

the conventional divertor approach is that of impurity contamination of the core plasma. This approach requires that central dilution is sufficiently low and that the radiated power losses are localized towards the plasma edge where fusion reactivity is lower. Advanced divertors, on the other hand, have the potential to decrease more the peak divertor heat than conventional divertor. This is achieved in part by specific features of the divertor magnetic geometry that enhance spreading of the power flux by diffusion and by increasing the volume for plasma radiation to occur and/or its stability so that the radiation remains located near the divertor targets. Research on advanced divertors is at a rather early stage and it remains to be demonstrated which of their potentialities will be materialized and which ones not because of limitations of divertor performance caused by physics and because of compatibility issues with high confinement plasmas. It may be well the case that the final solution to the DEMO power exhaust challenge counts with elements from both the conventional divertor approach (i.e. increased core radiation levels) and the advanced divertor approach.

Specific questions where some advanced divertor concepts may find issues of complex resolution concern power exhaust during confinement transients and in ELM suppressed regimes by 3-D fields as well as in reconciling the requirements for power exhaust and particle exhaust (including Helium exhaust) simultaneously. While these issues are of complex resolution also for the conventional divertor, viable approaches to meet the requirements exist and have been demonstrated experimentally and modelled for ITER. It is important that such important issues are considered early in the research programme for advanced divertor concepts.

Acknowledgement. ITER is the Nuclear Facility INB no. 174. The views and opinions expressed herein do not necessarily reflect those of the ITER Organization. This work has been carried out within the framework of the EUROfusion Consortium and has received funding from the Euratom research and training programme 2014-2018 under grant agreement No 633053. The views and opinions expressed herein do not necessarily reflect those of the European Commission.

6. References

[Ahn 2014] J.W. Ahn, et al., 2014 Plasma Phys. Control. Fusion **56** 015005.

[Angioni 2014] C. Angioni, et al., 2014 Nucl. Fusion **54** 083028.

[Angioni 2017a] C. Angioni, et al., 2017 Nucl. Fusion **57** 022009.

[Angioni 2017b] C. Angioni, et al., accepted for publication in Nucl. Fusion, 2017.

[Baylor 2013] L.R. Baylor, et al., 2013 Phys. Rev. Lett. **110** 245001.

[Borrass 1997] K. Borrass, et al., 1997 J. Nucl. Mater. **241-243** 250.

[Carralero 2015] D. Carralero, et al., 2015 Phys. Rev. Lett. **115** 215002.

[Chankin 2014] A. V. Chankin, et al., 2014 Plasma Phys. Control. Fusion **56** 025003.

[Den Harder 2016] N. Den Harder, et. Al., 2016 Nucl. Fusion **56** 026014.

[Dux 2011] R. Dux, et al., 2011 Nucl. Fusion **51** 053002.

[Dux 2014a] R. Dux, et al., 2014 Plasma Phys. Control. Fusion **56** 124003.

[Dux 2014b] R. Dux, et al., Proc. 24th IAEA Fusion Energy Conference, St. Petersburg, Russia, 2014. Paper TH/P3-29.

[Dunne 2017] M. G. Dunne, et al., 2017 Plasma Phys. Control. Fusion **59** 014017.

[Eich 2013] T. Eich, et al., 2013 Nucl. Fusion **53** 093031.

[Eich 2017] T. Eich, et al., to be published in Nuclear Materials and Energy, 2017.

[Garofalo 2015] A.M. Garofalo, 2015 Physics of Plasmas **22** 056116.

[Giroud 2013] C. Giroud, et al., 2013 Nucl. Fusion **53** 113025.

[Goldston 2012] R.J. Goldston, 2012 Nucl. Fusion **52** 013009.

[Greenwald 2002] M. Greenwald, Plasma Phys. Control. Fusion **44** (2002) R27-R53.

[Greenwald 2004] M. Greenwald, et al., 2014 Physics of Plasmas **21** 110501.

[Groth 2002] M. Groth, et al., 2002 Nucl. Fusion **42** 591.

[Guillemaut 2017] C. Guillemaut, et al., 2017 Plasma Phys. Control. Fusion **59** 045001.

[Hatch 2017] D.R. Hatch, et al., 2017 Nucl. Fusion **57** 036020.

[Havlíčková 2014] E. Havlíčková, et al., 2014 Plasma Phys. Control. Fusion **56** 075008.

[Hirai 2013] T. Hirai, et al., 2013 Fusion Engineering and Design **9–10** 1798.

[Horton 1999] L.D. Horton, et al., 1999 Nucl. Fusion **39** 993.

[Hubbard 2016] A.E. Hubbard, et al., 2016 Nucl. Fusion **56** 086003.

[Hughes 2011] J.W. Hughes, et al., 2011 Nucl. Fusion **51** 083007.

[ITER Physics Basis 2007] ITER Physics Basis editors, 2007 Nucl. Fusion **47** S1.

[Kallenbach 2005] A. Kallenbach, et al., 2005 Plasma Phys. Control. Fusion **47** B207.

[Kallenbach 2013] A Kallenbach, et al., 2013 Plasma Phys. Control. Fusion 55 124041.

[Kallenbach 2015] A. Kallenbach, et al., 2015 Nucl. Fusion **55** 053026.

[Kotschenreuther 2013] M. Kotschenreuther, et al., Physics of Plasmas **20** 102507 (2013).

[Kukushkin 2005] A.S. Kukushkin, et al., 2005 Nucl. Fusion 45 608.

[Kukushkin 2009] A.S. Kukushkin, et al., 2009 Nucl. Fusion **49** 075008.

[Kukushkin 2013] A. Kukushkin, et al., Jour. Nucl. Mat. **438** (2013) S203.

[Koechl 2016] F. Koechl, et al. submitted to Nucl. Fusion, 2016.

[LaBombard 1995] B. LaBombard, B., et al., Phys. Plasmas **2** (1995) 2242.

[Lang 2013] P.T. Lang, et al., 2013 Nucl. Fusion **53** 043004.

[Li 2013] J. Li, et al., 2013 Nature Physics **9** 817.

[Lisgo 2005] S. Lisgo, et al., Journal of Nuclear Materials **337** 139.

[Loarte 1998] A. Loarte, et al., 1998 Nuclear Fusion **38** 331.

[Loarte 2001] A. Loarte, et al., 2001 Plasma Phys. Control. Fusion **43** R183.

[Loarte 2014a] A. Loarte, et al., 2014 Nucl. Fusion **54** 123014.

[Loarte 2014b] A. Loarte, et al., 2014 Nucl. Fusion **54** 033007.

[Loarte 2008] A. Loarte, Proc. 22nd IAEA Fusion Energy Conference, Geneva, Switzerland, 2008. Paper IT/P6-13.

[Loarte 2015a] A. Loarte, et al., Journal of Nuclear Materials **463** (2015) 401.

[Loarte 2015b] A. Loarte, et al., 2015 Physics of Plasmas **22** 056117.

[Martin 2008] Y. Martin, et al., Journal of Physics: Conference Series **123** (2008) 012033.

[Mantica 2013] P. Mantica, et al., Proc. 40th EPS Conference on Plasma Physics, Espoo, Finland, 2013.

[Mazitelli 2015] G. Mazzitelli, et al., 2015 Nucl. Fusion **55** 027001.

[Merola 2002] M. Merola, et al., 2002 Journal of Nuclear Materials **307–311** (Part 2) 1524.

[Militello-Asp 2016] E. Militello-Asp, Proc. 26th IAEA Fusion Energy Conference, Kyoto, Japan, 2016. Paper TH/P2-23.

[McCracken 1993] G. M. McCracken, et al., 1993 Plasma Phys. Control. Fusion **35** 253.

[Monk 1996] R.D. Monk, PhD thesis, University of London (1996).

[Monk 1997] R.D. Monk, et al. 1997 Controlled Fusion and Plasma Physics, Proc. 24th Eur. Conf. (Berchtesgaden) vol 21A, part I (Geneva: European Physical Society) p 117.

[Mertens 2000] V. Mertens, et al., 2000 Nucl. Fusion **40** 1839.

[Neu 2005] R. Neu, et al., 2005 Nucl. Fusion **45** 209.

[Petrie 1997] T.W. Petrie, et al., 1997 Nucl. Fusion **37** 321.

[Pitts 2013] R.A. Pitts, et al., Journal of Nuclear Materials **438** (2013) S48.

[Polevoi 2016] A.R. Polevoi, et al., Proc. 26th IAEA Fusion Energy Conference, Kyoto, Japan, 2016. Paper EX/P6-44.

[Rapp 2009] J. Rapp, et al., 2009 Nucl. Fusion **49** 095012.

[Reimerdes 2013] H. Reimerdes, et al., 2013 Plasma Phys. Control. Fusion **55** 124027.

[Romanelli 2013] F. Romanelli, et al., 2013 Nucl. Fusion **53** 104002.

[Romanelli 2015] M. Romanelli, et al., 2015 Nucl. Fusion **55** 093008.

[Roth 2008] J. Roth, et al., 2008 Plasma Phys. Control. Fusion **50** 103001.

[Schmitz 2016] O. Schmitz, et al., 2016 Nucl. Fusion **56** 066008.

[Soukhanovskii 2015] V.A. Soukhanovskii, et al., Journal of Nuclear Materials **463** (2015) 1191.

[Stangeby 1993] P.C. Stangeby, 1993 Nucl. Fusion **33** 1695.

[Strachan 1997] J. D. Strachan, et al., 1997 Plasma Phys. Control. Fusion **39** B103.

[Wagner 1982] F. Wagner, et al., Phys Rev Lett (1982) **49** 1408.

[Wenninger 2015] R. Wenninger, et al., 2015 Nucl. Fusion **55** 063003.

[Wenzel 1999] U. Wenzel. et al., 1999 Nucl. Fusion **39** 873.

[Wischmeier 2015] M. Wischmeier, et al., 2015 Journal of Nuclear Materials **463** 22.